PHYSICAL REVIEW D VOLUME 26, NUMBER 5 1 SEPTEMBER 1982

Hadron production by e^+e^- annihilation at center-of-mass energies between 2.6 and 7.8 GeV. II. Jet structure and related inclusive distributions

G. Hanson, M. S. Alam,[a] A. M. Boyarski, M. Breidenbach, F. Bulos,
J. T. Dakin,[b] J. M. Dorfan, G. J. Feldman, G. E. Fischer, D. Fryberger, D. L. Hartill,[c]
J. A. Jaros, B. Jean-Marie,[d] R. R. Larsen, V. Lüth,
H. L. Lynch,[e],[f] D. Lyon,[g] C. C. Morehouse,[h] J. M. Paterson, M. L. Perl,
I. Peruzzi,[i] M. Piccolo,[i] T. P. Pun,[j] P. Rapidis,[k] B. Richter,
R. H. Schindler,[l] R. F. Schwitters,[m] J. L. Siegrist,[l] W. Tanenbaum,[n] and F. Vannucci[o]
Stanford Linear Accelerator Center, Stanford University, Stanford, California 94305

G. S. Abrams, D. Briggs,[f] W. C. Carithers, W. Chinowsky, S. Cooper,[e]
R. G. DeVoe,[p] C. E. Friedberg,[q] G. Goldhaber, R. J. Hollebeek,[r]
A. D. Johnson, J. A. Kadyk, A. M. Litke,[s] R. J. Madaras, H. K. Nguyen,[t]
F. M. Pierre,[u] B. Sadoulet,[l] G. H. Trilling, J. S. Whitaker,[v] F. C. Winkelmann, and J. E. Wiss[w]
Lawrence Berkeley Laboratory and Department of Physics,
University of California, Berkeley, California 94720
(Received 12 April 1982)

We present results on the jet structure observed in multihadronic events produced by e^+e^- annihilation in the Mark I magnetic detector at SPEAR. The evidence for jet structure and the jet-axis angular distribution are reported. We give inclusive distributions of the hadrons in Feynman x, rapidity, and transverse momentum relative to the jet axis.

I. INTRODUCTION

In the preceding paper[1] (hereafter referred to as I) we presented results on the total cross section and inclusive momentum distributions for multihadronic events produced by e^+e^- annihilation in the center-of-mass energy ($E_{\text{c.m.}}$) range from 2.6 to 7.8 GeV from the Mark I magnetic detector at SPEAR. In this paper we present results on the jet structure observed in these events.

In e^+e^- collisions the electron and positron predominantly annihilate to form a single virtual photon which subsequently produces a lepton-antilepton pair (e.g., $\tau^+\tau^-$), or a quark-antiquark pair which converts into hadrons. At sufficiently high energy the multihadronic events produced by e^+e^- annihilation are expected to form two back-to-back jets due to the limiting of transverse momentum along the original quark direction.[2–5] The spins of the quarks can be determined from the jet-axis angular distribution. Evidence for such jet structure was first observed at SPEAR for $E_{\text{c.m.}}$ of 4.8 GeV and greater.[6] If the jet structure is due to quark jets, then it is of interest to study inclusive distributions of hadrons relative to the jet direction in order to obtain information about the fragmentation of quarks into hadrons. In this paper we present hadron inclusive distributions in Feynman x, rapidity, and transverse momentum relative to the jet direction in multihadronic events from e^+e^- annihilation in the $E_{\text{c.m.}}$ range from 3.0 to 7.8 GeV.

As in I we limit ourselves to data away from the ψ resonances[7] and restrict ourselves even further to data away from the charm-threshold region.[8] The apparatus, trigger criteria, general analysis procedures, hardronic-event selection, luminosity measurement, and general Monte Carlo calculation of detector efficiency are described in I. We shall give a complete report on the jet-structure analysis. The evidence for jet structure is presented in Sec. II. Section III describes the measurement of the jet-axis angular distribution. The determination of inclusive distributions in variables relative to the jet direction is the subject of Sec. IV.

II. EVIDENCE FOR JET STRUCTURE

One of the most definitive predictions of quark-parton constituent models of elementary particles

is that the hadrons produced in e^+e^- annihilation should form back-to-back jets.[2–5] The e^+ and e^- annihilate to form a single virtual photon which produces a quark-antiquark pair, each of which fragments to hadrons, as shown in Fig. 1. The jet structure arises from the limiting of transverse momentum of the hadrons relative to the original parton direction and should become apparent at energies high enough that the total momentum of the hadrons is large compared with the fundamental transverse momentum limitation. The original quark-pair angular distribution is expected to be the same as for any pair of spin-$\frac{1}{2}$ particles: $1+\cos^2\theta$, where θ is the polar angle relative to the e^+ beam direction.

In searching for jet structure in multihadronic events produced in e^+e^- annihilation, one is faced with two fundamental problems:

(1) If there is a direction relative to which transverse momentum is limited, what is that direction for a particular event?

(2) If the transverse momentum is indeed limited, what is the measure of that limitation?

In addition, there are problems caused by detection inefficiencies. Charged particles were measured over only 65% of 4π sr in the Mark I detector, described in I. Neutral particles were detected with significantly worse efficiency and resolution than charged particles and were not used in this analysis. Multihadronic events were almost never fully reconstructed.

The procedure[9] which was used[6,10] to solve these problems will now be described. First, we find the direction which minimizes the sum of squares of transverse momenta for each event. To do this, we diagonalize the tensor

$$T^{\alpha\beta}=\sum_i (\delta^{\alpha\beta}\vec{p}_i{}^2-p_i^\alpha p_i^\beta)\ , \tag{2.1}$$

where the summation is over all detected charged particles and α and β refer to the spatial components of each particle momentum $\vec{p}_i$. Since $T^{\alpha\beta}$ is like a moment-of-inertia tensor, we are finding principal moments in momentum space. We obtain the eigenvalues λ_1, λ_2, and λ_3 which are the sums of squares of transverse momenta with respect to the three eigenvector directions. The smallest eigenvalue λ_3 is the minimum sum of squares of transverse momenta, and the eigenvector direction associated with it is the reconstructed *jet axis.* This method of calculating the jet axis is not perfect. It is impossible to determine the jet axis exactly, even with perfect detection, unless one knows precisely which particle comes from which jet, in which case one could simply find the resultant momenta of two groups of particles. Using Monte Carlo simulations of the detector and jet models in which the true jet axis was known for each event, we have studied other methods for finding the jet axis, such as maximizing the sum of the absolute values of the longitudinal momenta, and have found that the method described above is the best approximation of which we are aware. The median angle between the true jet axis and the reconstructed jet axis for hadronic events with three or more prongs in the Mark I detector at 7.3 GeV was estimated to be 24°. The method also has the advantage that it is a well-defined mathematical procedure which can be applied to any detected event or to events generated by any Monte Carlo model and which does not use large amounts of computer time.

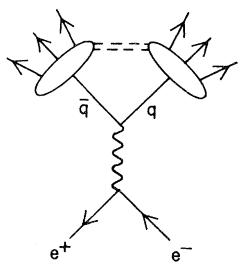

FIG. 1. Hadron production by e^+e^- annihilation in quark-parton model.

A jet axis can be determined for any event regardless of whether it is jetlike. Once the jet axis is determined, we obtain a quantitative measure of how jetlike an event is from the *sphericity (S):*

$$S=\frac{3\lambda_3}{\lambda_1+\lambda_2+\lambda_3}=\frac{3\left[\sum_i p_{\perp i}{}^2\right]_{\min}}{2\sum_i \vec{p}_i{}^2}\ . \tag{2.2}$$

The sphericity is the ratio of the minimum sum of squares of transverse momenta normalized to the sum of squares of total momenta. The sphericity approaches 0 for events with limited transverse momentum (jetlike events) and approaches 1 for events with large multiplicity and isotropic particle distributions.

Monte Carlo simulations were used to determine how jetlike hadronic events differ from isotropic hadronic events in the detector. The detector was simulated as described in I. Events were generated according to Lorentz-invariant phase space or a

limited-transverse-momentum jet model[11] in which phase space was modified by a matrix element squared of the form

$$M^2=\exp\left[-\left[\sum_i p_{\perp i}^2\right]/2b^2\right], \tag{2.3}$$

where $p_{\perp i}$ is the momentum perpendicular to the jet axis for the ith particle and b is a parameter chosen to fit the data. The sum is over all produced particles. The assumed jet-axis angular distribution was of the form

$$\frac{d\sigma}{d\Omega}\propto 1+\alpha\cos^2\theta\,. \tag{2.4}$$

We used $\alpha=1$ in agreement with the measurement of the jet-axis angular distribution which is described in detail in Sec. III. Generated events had only pions with the charged and neutral multiplicities given by separate Poisson distributions as in I. Initial-state radiation was included in the production of the events. Some specific checks were performed using models which included production of η's, kaons, and nucleons.

Multihadronic events were selected as described in I. For this analysis we used only those events with three or more observed tracks in order to reduce the contamination from beam-gas interactions, two-photon processes, and $\tau^+\tau^-$ production. Additional cuts were applied as in I to remove multiprong events originating from QED processes (mainly Bhabha-scattering events containing a δ ray or converted photon). These cuts are particularly important for the jet analysis because they selectively reduce background in events containing a track with momentum near the beam energy; these events are relatively rare in multihadronic processes. Contamination of this event sample is estimated to range from 1% for $E_{\text{c.m.}}=3$ GeV to 4% for $E_{\text{c.m.}}>7$ GeV from beam-gas interactions, to be $<2\%$ from two-photon processes, and to be $\lesssim 7\%$ from $\tau^+\tau^-$ production. We used the large blocks of data collected at $E_{\text{c.m.}}$ of 3.0, 4.8, 6.2, and 7.4 GeV, which consisted of 1100, 7300, 6800, and 14 500 multihadronic events, respectively, after cuts. From I we recall that 3.0 GeV is below the threshold for production of charmed quarks and the other energies are above.

The data at each energy were compared with Monte Carlo simulations based on either the phase-space model or the jet model. At each energy the total multiplicity and ratio of charged pions to neutral pions for both models were obtained by fitting to the observed charged particle mean momentum and mean multiplicity. The parameter b in Eq. (2.3) was chosen by fitting to the observed mean $p_\perp$ with respect to the observed jet axis. The observed distribution of $p_\perp$ at 7.4 GeV is shown in Fig. 2 along with the predictions of the two models. The jet model reproduces the data rather well whereas phase space predicts too many particles at high $p_\perp$. The mean produced $p_\perp$ in the jet model was found to be in the range 325 to 360 MeV/c with no particular energy dependence. From hadron-interaction data we would have expected the mean $p_\perp$ to be in the range 300 to 350 MeV/c.

The observed sphericity distributions were compared with the predictions of the two models. Figure 3 shows the observed S distributions for the lowest energy, 3.0 GeV, and for the two highest energies, 6.2 and 7.4 GeV. At 3.0 GeV the data agree with the predictions of either the phase-space model or the jet model. At this energy the limiting of transverse momentum to an average of 350 MeV/c has no effect on the phase-space particle distributions as manifested in the S distribution since the predictions of the two models are the same. At 6.2 and 7.4 GeV the S distributions are peaked toward low S favoring the jet model over the phase-space model. At the highest energies the two larger eigenvalues λ_1 and λ_2 are nearly equal.

Figure 4 shows the observed S distribution at 7.4 GeV compared with the predictions of both a jet

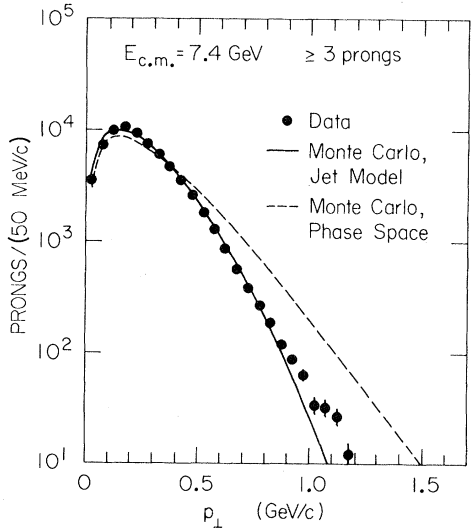

FIG. 2. Observed single-particle $p_\perp$ with respect to jet axis for events with three or more detected charged particles for 7.4-GeV data compared with the jet model (solid curve) and phase-space model (dashed curve) predictions.

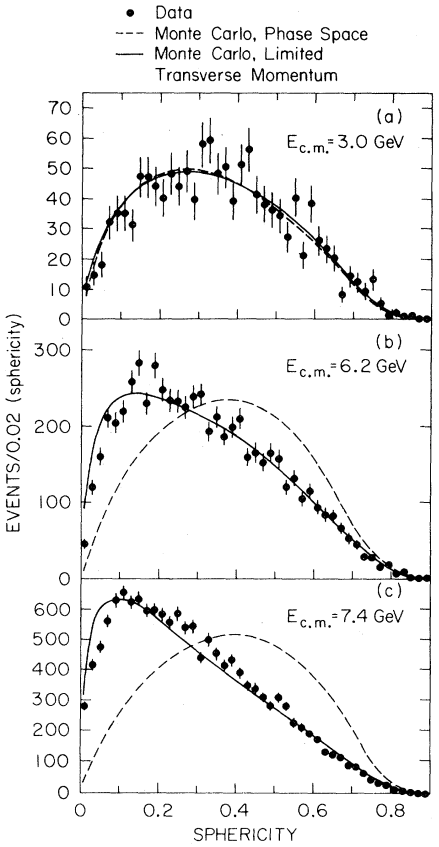

FIG. 3. Observed sphericity distributions for data, jet model (solid curves), and phase-space model (dashed curves) for (a) $E_{c.m.}=3.0$ GeV, (b) $E_{c.m.}=6.2$ GeV, and (c) $E_{c.m.}=7.4$ GeV.

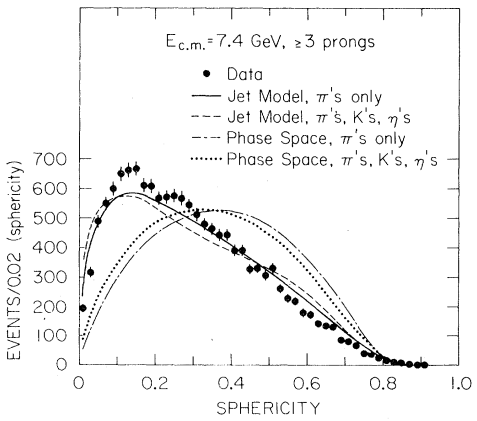

FIG. 4. Observed sphericity distribution at 7.4 GeV compared with prediction for jet model with pions only (solid curve), jet model with pions, kaons, and η's (dashed curve), phase-space model with pions only (dashed-dotted curve), and phase-space model with pions, kaons, and η's (dotted curve).

model and a phase-space model in which kaons and η's were produced along with pions. η's and π^0's were produced with equal probability before phase-space effects, and kaon fractions were fitted to agree with the data.[12]

The agreement of the observed sphericity distributions with the jet model as opposed to the phase-space model is evidence for jet structure in e^+e^- hadron production. Differences in the detailed shape of the S distributions between the data and the jet model can be caused by differences in the shape of the multiplicity distributions (see Fig. 15 in I) and interparticle correlations caused by decaying resonances and particles.

The difference between the jet model and phase-space model predictions for sphericity as a function of energy can be seen quantitatively in Fig. 5 which shows the observed mean S versus $E_{c.m.}$. The phase-space model predicts that the mean S should increase as $E_{c.m.}$ increases whereas the jet model predicts that the mean S should decrease. The data clearly show a decreasing mean S with increasing $E_{c.m.}$ consistent with the jet model.

The evidence for jet structure is corroborated by the distributions of the cosine of the angle between any pair of particles, shown in Fig. 6. At 6.2 and 7.4 GeV the data show more pairs of particles at small angles to each other and at angles near 180° to each other than the phase-space model predicts.

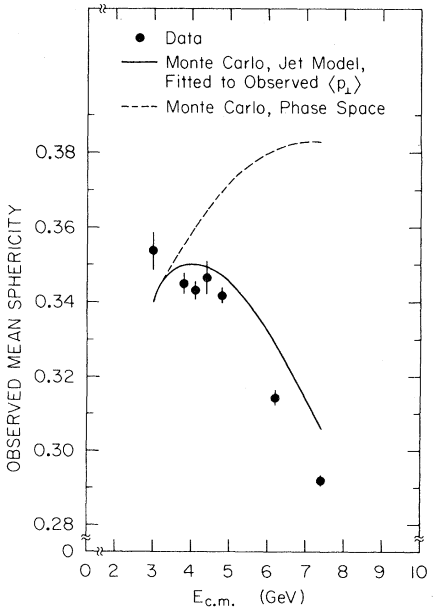

FIG. 5. Observed mean sphericity vs $E_{c.m.}$ for data, jet model (solid curve), and phase-space model (dashed curve).

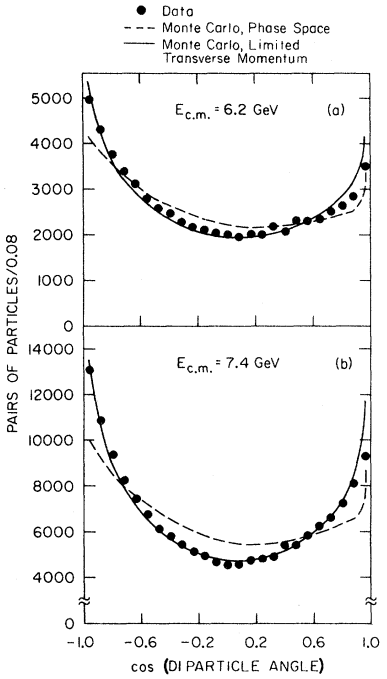

FIG. 6. Distributions of the cosine of diparticle angles for data, jet model (solid curves), and phase-space model (dashed curves) for (a) $E_{c.m.} = 6.2$ GeV and (b) $E_{c.m.} = 7.4$ GeV.

The distributions agree well with the jet model.

Further corroboration for the jet model can be found in the observed single-particle inclusive x distribution presented in Fig. 7 for events at 7.4 GeV. (x is the scaling variable $2p/E_{c.m.}$, where p is the particle momentum.) The jet model reproduces this distribution quite well whereas the phase-space model predicts too few particles with $x \gtrsim 0.4$. However, one could argue that the reason the S distributions agree with the jet model is that the jet model produces a larger number of events with high momentum particles and such events tend to have low S. To determine whether the agreement of the S distributions is simply a consequence of the agreement of the x distributions, we examined the S distributions for those events in which no particle has $x > 0.4$. For these events the x distributions for both models agree with the data. The S distributions for such events at 7.4 GeV are shown in Fig. 8(a). The jet model is still preferred over the phase-space model. The S distributions for events having a particle with $x > 0.4$ are shown in Fig. 8(b). Although the agreement is not perfect, the data are definitely in better agreement with the jet model. Therefore we conclude that the agreement of the S distributions with the jet model is not due simply to the agreement of the x distributions and, furthermore, the agreement of the x distributions is a consequence of the jet structure. In fact, in the jet model the production of high-momentum particles is directly related to the limiting of transverse momentum relative to an axis.

Another possible cause for the appearance of jet structure is the production of resonances or new

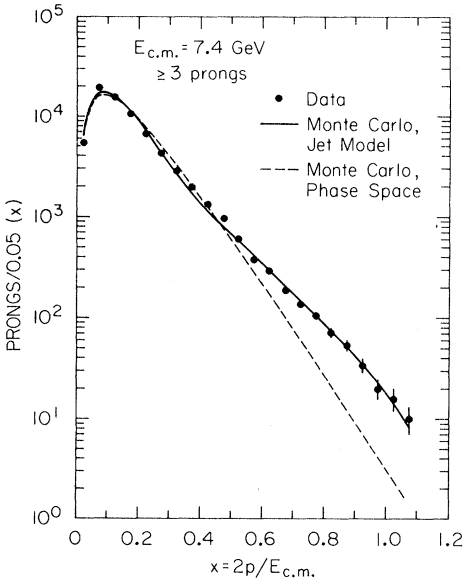

FIG. 7. Observed single-particle x distribution for events with three or more detected charged particles at 7.4 GeV compared with the jet model (solid curve) and phase-space model (dashed curve) predictions.

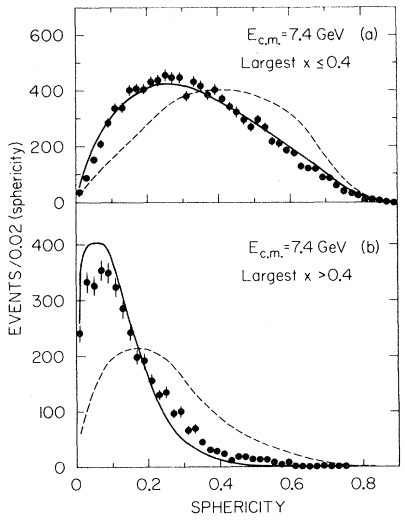

FIG. 8. Observed sphericity distributions at 7.4 GeV for data, jet model (solid curves), and phase-space model (dashed curves) for (a) events with largest $x \leq 0.4$ and (b) events with largest $x > 0.4$.

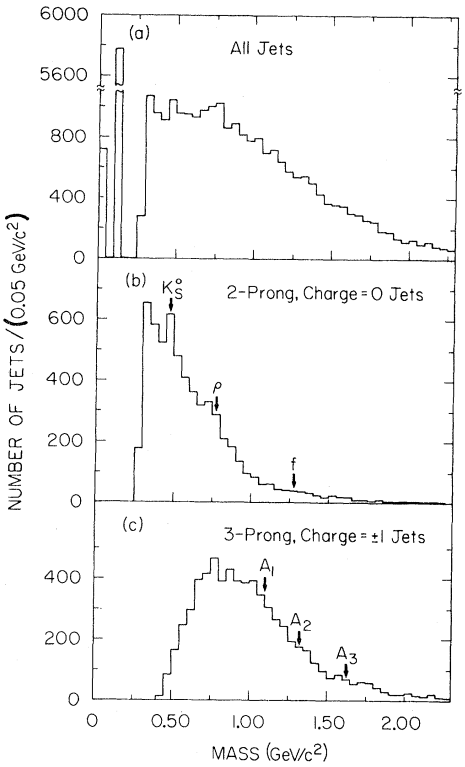

FIG. 9. Observed jet mass distributions at 7.4 GeV for (a) all jets, (b) two-prong, charge=0 jets, and (c) three-prong, charge=±1 jets. Pion masses were used for all particles. The arrows indicate the masses of particles or resonances having the indicated decay modes.

particles. In order to search for jets which are actually the decays of particles or resonances we examined the distributions of observed masses of jets as shown in Fig. 9 for 7.4 GeV data. The jet mass is the effective mass of all detected particles in an event on one side of a plane through the interaction vertex and perpendicular to the jet axis. Pion masses were used for all particles. Figure 9(a) shows the mass distribution for all jets. The spikes at masses of zero and the pion mass are due to zero-particle and one-particle jets, respectively. Most jet masses are less than 2 GeV/c^2. Figure 9(b) shows the mass distribution for two-prong, charge=0 jets. One can see that some jets are K_S^0's and that there is a shoulder at the ρ^0 mass. There is no evidence for the f^0. There is no evidence for any structure in the mass distribution for three-prong, charge=±1 jets, shown in Fig. 9(c). We conclude that there is no evidence for copious production of resonances which could lead to jet structure in the majority of the events. However, neutral particles are not detected and are therefore not included in the mass calculations. The effects of charmed-particle production are not evident from these distributions and will be discussed further in Sec. IV.

The evidence for jet structure is statistical; that is, single events cannot be interpreted as either jetlike or isotropic. Events produced from the jet model Monte Carlo simulation can appear to be of either type. In the SPEAR energy range the limitation of transverse momentum to ~350 MeV/c, is not enough to make jets obvious. However, for the purposes of illustration, we show in Fig. 10 a sample 7.4-GeV event: a "typical" jetlike event. The reconstructed jet axis is shown. The event has eight tracks, two of which have $x > 0.3$. The other six tracks have low momentum. The event has $S=0.081$. The observed energy is less than $E_{\text{c.m.}}$ and the momenta do not balance, so there are missing particles.

III. MEASUREMENT OF JET-AXIS ANGULAR DISTRIBUTION

In quark-parton models the angular distribution of the jet axis is determined by the angular distri-

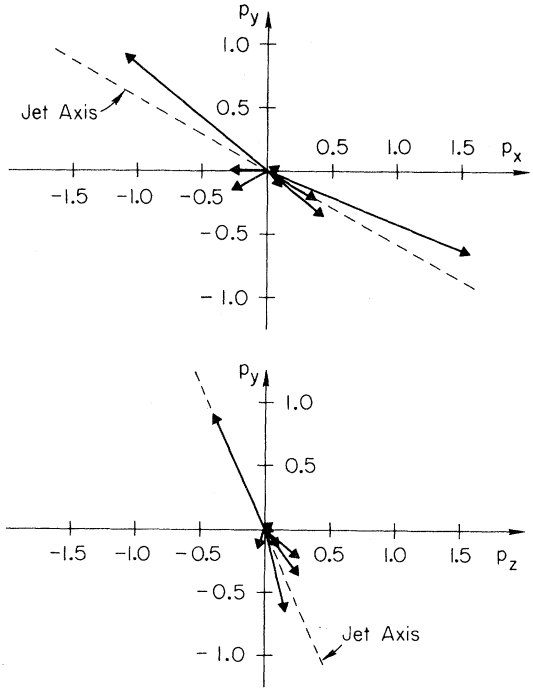

FIG. 10. Momentum-space representation of a sample 7.4-GeV event. p_x, p_y, p_z refer to the three spatial components of the particle momenta. The z axis lies along the positron direction. This event has eight tracks, two with $x > 0.3$. The reconstructed jet axis is represented by the dashed line. The event has $S=0.081$.

bution of the original quark pair. Thus the spins of the quarks can be inferred from a measurement of this angular distribution. The most general angular distribution for production of any quarks or particles through a single virtual photon is[13]

$$\frac{d\sigma}{d\Omega}=\tfrac{1}{2}(\sigma_T+\sigma_L)[1+\alpha\cos^2\theta + P^2\alpha\sin^2\theta\cos2\phi], \quad (3.1)$$

where θ is the polar angle of the particle with respect to the e^+ beam direction, ϕ is the azimuthal angle with respect to the (horizontal) plane of the storage ring, and P is the degree of transverse polarization of each beam. The quantity α is given by

$$\alpha=\frac{\sigma_T-\sigma_L}{\sigma_T+\sigma_L}, \quad (3.2)$$

where σ_T and σ_L are the transverse (helicity ±1 along the particle direction) and longitudinal (helicity 0 along the particle direction) production cross sections. For the production of a pair of spin-$\frac{1}{2}$ particles, for example, the QED reaction $e^+e^-\to\mu^+\mu^-$, $\alpha=1$. For a pair of spin-0 particles $\alpha=-1$. For multihadron production, α is bounded between these two extreme values and depends, in general, on $E_{\text{c.m.}}$ and the particle type and momentum. [The same expression in different form is given by Eq. (1.2) in I where the single-particle inclusive cross section is discussed.]

The transverse-polarization term in Eq. (3.1) does not provide any new information that could not be obtained by measuring the polar angle dependence alone. However, the detector had a limited acceptance in polar angle (50° to 130°) but had a full 2π azimuthal acceptance. The existence of transverse beam polarization thus allowed a more precise measurement of the jet-axis angular distribution from the azimuthal angle distribution alone. Use of the ϕ distribution for the jet axis was more important than for the case of single-particle inclusive distributions because in the latter case the acceptance cuts off fairly cleanly at the polar-angle edge of the detector whereas in the former case the jet-axis polar-angle distribution is smeared by the additional complication of the jet-axis determination.

In high-energy e^+e^- storage rings the beams become transversely polarized under certain conditions through the mechanism of synchrotron radiation with spin flip.[14] This is called radiative beam polarization and was first discussed by Ternov, Loskutov, and Korovina in 1961.[15] The amount of spin-flip radiation is extremely small compared with the ordinary (nonflip) synchrotron radiation. In 1963 Sokolov and Ternov[16] showed that for initially unpolarized electrons or positrons of charge e, mass m, and energy $E=\gamma mc^2$ in uniform motion in a circle of radius ρ there is a gradual buildup of transverse polarization according to

$$P(t)=\frac{8\sqrt{3}}{15}(1-e^{-t/\tau_0}), \quad (3.3)$$

where the characteristic time τ_0 is given by

$$\frac{1}{\tau_0}=\frac{5\sqrt{3}}{8}\frac{e^2\hbar\gamma^5}{m^2c^2\rho^3}. \quad (3.4)$$

Positrons are polarized parallel to the magnetic field, electrons antiparallel. For a storage ring consisting of a set of identical bending magnets of bending radius ρ and straight sections combining to an orbit of circumference $2\pi R$, a convenient formula for the polarization time constant is

$$\tau_0(\text{sec})=98.7\frac{[\rho(M)]^3}{[E(\text{GeV})]^5}\frac{R}{\rho}. \quad (3.5)$$

The most distinctive feature of Eq. (3.5) is the very strong energy dependence. At SPEAR the polarization time constant is approximately 14 min at 3.7 GeV per beam.

The transverse beam polarization was observed to reach about 80% of the expected maximum value at $E_{\text{c.m.}}=7.4$ GeV.[17] The resulting azimuthal asymmetries were used to determine the jet-axis angular distribution and the single-particle inclusive angular distributions for multihadronic events. The data from $e^+e^-\to\mu^+\mu^-$ taken simultaneously with the multihadron data at 7.4 GeV were used to determined a time-average value of $P^2=0.47\pm0.05$.

Figure 11 shows the observed jet-axis ϕ distributions for jet axes with $|\cos\theta|\le0.6$ for 6.2 and 7.4 GeV data. (Since the jet axis is a symmetry axis, the angle $\phi+180°$ is equivalent to the angle ϕ.) At 6.2 GeV, where the beam energy corresponds to a spin-depolarization resonance, the ϕ distribution is flat. The 6.2-GeV data were used to check that there was no ϕ asymmetry introduced by the detector. At 7.4 GeV a strong azimuthal dependence is observed.[6,10] The ϕ distribution shows an asymmetry with maxima and minima at the same values of ϕ as for $e^+e^-\to\mu^+\mu^-$.

The observed jet-axis ϕ asymmetry at 7.4 GeV and the measured value of P^2 were used to determine the parameter α for the jet-axis angular distribution as given by Eq. (3.1). The observed value

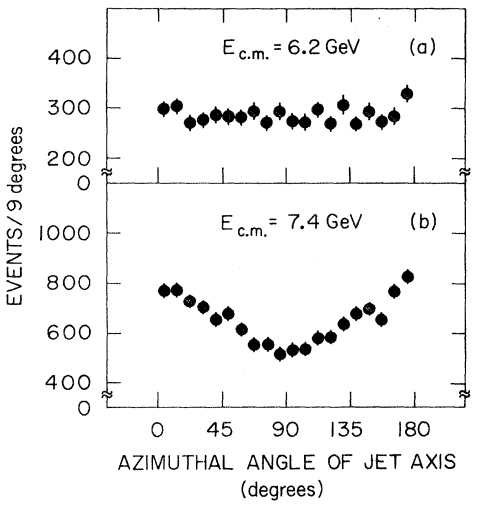

FIG. 11. Observed distributions of jet-axis azimuthal angles from the plane of the storage ring for jet axes with $|\cos\theta| \leq 0.6$ for (a) $E_{\text{c.m.}} = 6.2$ GeV and (b) $E_{\text{c.m.}} = 7.4$ GeV.

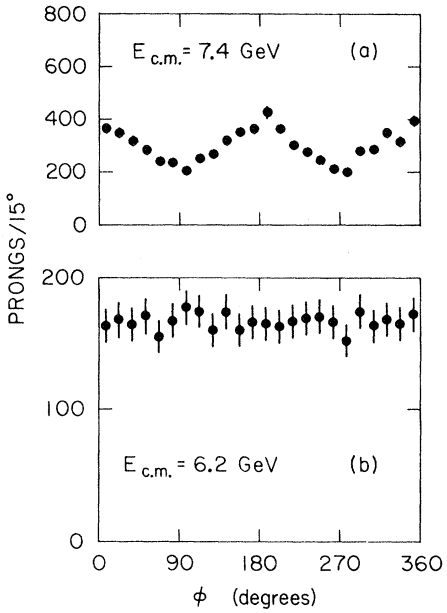

FIG. 12. Observed single-particle inclusive distributions in azimuthal angle ϕ for particles with $x > 0.3$ and $|\cos\theta| \leq 0.6$ for (a) $E_{\text{c.m.}} = 7.4$ GeV and (b) $E_{\text{c.m.}} = 6.2$ GeV.

of α for the jet axis is $\alpha = 0.50 \pm 0.07$. From the jet-model Monte Carlo simulation, which included the angular distribution for the produced jet axis as in Eq. (3.1), we found that the observed value of α is less than the true value of α which describes the production of the jets because of the incomplete acceptance of the detector, the loss of neutral particles, and our method of reconstructing the jet axis. The simulation was used to calculate a ratio of observed to produced values of α of 0.52 at 7.4 GeV. This ratio was then used to correct the observed α to obtain $\alpha = 0.97 \pm 0.14$ for the produced jet-axis angular distribution. In terms of σ_L and σ_T this value of α corresponds to $\sigma_L/\sigma_T = 0.02 \pm 0.07$. The error in α is statistical only; we estimate that the systematic errors in the observed α can be neglected. The systematic error due to model dependence in the correction factor relating the observed to the produced values of α is expected to be small compared to the statistical error. The jet-axis angular distribution was thus found to be consistent with that for a pair of spin-$\frac{1}{2}$ particles, as predicted for jets originating from quarks.

An azimuthal asymmetry was also observed[18] in the single-particle inclusive ϕ distributions for the same sample of data at 7.4 GeV, as shown in Fig. 12 for particles with $x > 0.3$ and $|\cos\theta| \leq 0.6$. Again the asymmetry is observed to have the same sign as for μ-pair production. This observation is not surprising since the particles in these events were used to calculate the jet axis. The effect is momentum dependent in that the highest-momentum particles tend to follow the jet axis while the lowest-momentum particles are produced isotropically. The measured value of P^2 and the $\cos\theta$ and ϕ distributions of the particles as a function of x were used to determine the inclusive hadron α as a function of x. The jet-model Monte Carlo simulation was used to predict the single-particle angular distributions for all values of particle momenta. Figure 13 shows the values for the inclusive hadron α as a function of x at 7.4 GeV compared with the jet-model calculation. The model assumed the value $\alpha = 0.97 \pm 0.14$ for the jet-axis angular distribution. The prediction agrees well with the data for all values of x.

At energies other than 7.4 GeV it was not possible to make a precise determination of the jet-axis angular distribution because of the small beam polarization and consequent absence of ϕ asymmetry. The $\cos\theta$ distribution of the jet axis was too strongly affected by the limited acceptance of the detector in $\cos\theta$. We were able, however, to measure the inclusive hadron α versus x by fitting the inclusive $\cos\theta$ distributions. These determinations are less precise than those using polarized beams. Figure 14 shows best-fit values of α for various energies as a function of x. At 3.0 GeV the inclusive α distribution is constant with isotropy for all values of x. At the higher energies α begins to increase with increasing x beginning at $x \sim 0.3$ to

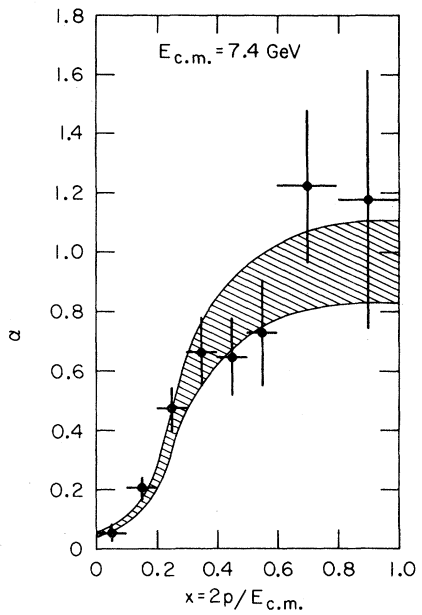

FIG. 13. Observed inclusive α vs x for particles with $|\cos\theta| \leq 0.6$ in hadronic events for $E_{c.m.} = 7.4$ GeV. The prediction of the jet-model Monte Carlo simulation for a jet-axis angular distribution with $\alpha = 0.97 \pm 0.14$ is represented by the shaded band.

maximum values near 1 at the higher values of x. These values are consistent with the polarized beam measurement. The jet-model simulation with a jet-axis angular distribution of $1 + \cos^2\theta$ can reproduce this dependence of α on x and $E_{c.m.}$ including the isotropy at 3.0 GeV. In fact, we begin

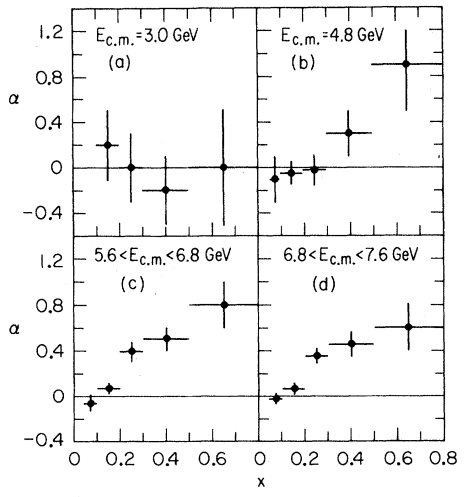

FIG. 14. Inclusive hadron angular distribution coefficient α vs x obtained from fits to $1 + \alpha(x)\cos^2\theta$ for (a) $E_{c.m.} = 3.0$ GeV, (b) $E_{c.m.} = 4.8$ GeV, (c) $5.6 < E_{c.m.} < 6.8$ GeV, and (d) $6.8 < E_{c.m.} < 7.6$ GeV.

to observe nonzero values for α at about the energies where jet structure begins to be differentiated from phase space.

The data strongly support a jet hypothesis for hadron production in e^+e^- annihilation. The jet-model Monte Carlo simulation reproduces not only the sphericity distributions for whole events but also the single-particle inclusive momentum and angular distributions. The jet-axis angular distribution integrated over azimuthal angle is proportional to $1 + (0.97 \pm 0.14)\cos^2\theta$ at 7.4 GeV, giving $\sigma_L/\sigma_T = 0.02 \pm 0.07$. The jet-axis angular distribution is consistent with that for a pair of spin-$\frac{1}{2}$ particles as expected in quark-parton models.

IV. INCLUSIVE DISTRIBUTIONS IN VARIABLES RELATIVE TO THE JET DIRECTION

We have seen that multihadronic events produced by e^+e^- annihilation exhibit jet structure as would be expected from a quark-pair origin. If the jet structure is indeed due to quark-parton jets, inclusive distributions in variables relative to the jet direction, which is expected to be the quark direction, will give information about the fragmentation of quarks into hadrons. One can study the dependence of the inclusive distributions in momentum transverse to the jet axis on the scaled momentum parallel to that axis. In addition, these inclusive distributions can be compared with similar distributions from other processes, such as leptoproduction and hadron-hadron interactions.

In order to investigate such questions we have measured inclusive distributions in Feynman x, rapidity, and transverse momentum relative to the jet axis. We have studied the biases which might be introduced by the methods used to measure these distributions. The jet-model Monte Carlo simulation was used to calculate corrections so that the distributions presented here are the best representations of the true distributions that we can measure given our knowledge of the detector and the production model.

For the measurement of inclusive distributions we used the multihadronic events with three or more detected charged particles at fixed $E_{c.m.}$ values of 3.0 and 4.8 GeV and in three energy ranges from 5.6 to 7.8 GeV. Although there is no differentiation between jet structure and isotropic production at 3.0 GeV, multihadronic events at that energy presumably occur via the production and fragmentation of quark-antiquark pairs. The

3.0-GeV data are therefore of use in providing a comparison with physics below charm threshold. The data samples consisted of 1100 events at 3.0 GeV, 7300 events at 4.8 GeV, 23 000 events from 5.6 to 6.3 GeV, 15 900 events from 6.3 to 7.0 GeV, and 51 900 events from 7.0 to 7.8 GeV after cuts had been applied.

We constructed the observed jet axis as described in Sec. II. The components of each particle momentum parallel to ($p_{||}$) and perpendicular to ($p_\perp$) the jet axis were then calculated, as shown in Fig. 15. We then produced observed inclusive distributions in $p_{||}$, $p_\perp$, and rapidity. The problem then was to correct these distributions for geometric acceptance, trigger bias, data analysis cuts, radiative corrections, and incorrect determination of the jet axis. Studies were made using the jet-model Monte Carlo simulation in which we knew the true jet axis for every event. It was found that the observed distributions in $p_{||}$ for all events were similar enough to the produced distributions that they could be corrected to give the true distributions. The rapidity and $p_\perp$ distributions, however, were more sensitive to the correct determination of the jet axis and could not be reasonably corrected without applying further event selection criteria. The method used for these distributions will be described later.

Since the inclusive quantity $s\,d\sigma/dx$ ($s=E_{\text{c.m.}}{}^2$), shown in Fig. 17(a) of I, nearly scales, we were led to examine the inclusive distributions for $s\,d\sigma/dx_{||}$, where $x_{||}$, or Feynman x, is defined by

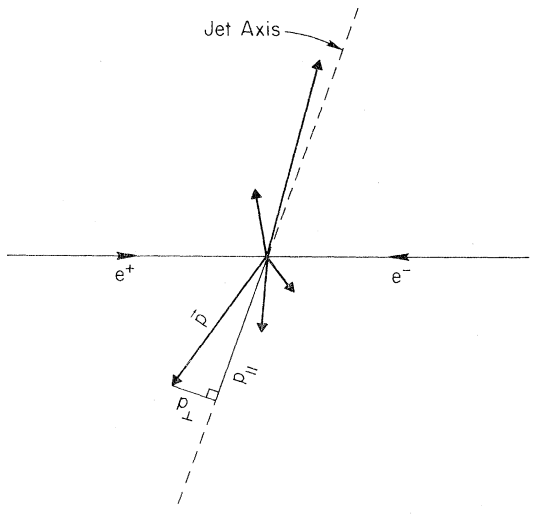

FIG. 15. Illustration of a hadronic event from e^+e^- annihilation showing the jet axis and the components of the momentum $\vec{p}$ of a particle parallel to ($p_{||}$) and perpendicular to ($p_\perp$) the jet axis.

$$x_{||}=2p_{||}/E_{\text{c.m.}}\ . \tag{4.1}$$

In quark-parton models $x_{||}$ is the fraction of parton momentum carried by the hadron in the direction of the parton.

The inclusive $s\,d\sigma/dx_{||}$ distribution is given for each $x_{||}$ bin by

$$s\frac{d\sigma}{dx_{||}}(x_{||i})=\frac{sN(x_{||i})}{\epsilon(x_{||i})L\,\delta x_{||i}}\ , \tag{4.2}$$

where $N(x_{||i})$ is the number of detected tracks in the bin centered on $x_{||}=x_{||i}$, L is the integrated luminosity for the data sample, $\delta x_{||i}$ is the bin width, and $\epsilon(x_{||i})$ is the single-particle inclusive detection efficiency determined from the Monte Carlo simulation for the $x_{||}$ bin centered at $x_{||i}$. The efficiency $\epsilon(x_{||i})$ is made up of several parts:

$$\epsilon(x_{||i})=\frac{N_D(x_{||i})}{N_P(x_{||_i})}\epsilon_v b(1+\delta)\ , \tag{4.3}$$

where $N_D(x_{||i})$ is the number of detected particles in the $x_{||}$ bin centered at $x_{||i}$ *in the Monte Carlo calculation* ($x_{||}$ is calculated relative to the observed jet axis), $N_P(x_{||i})$ is the number of produced particles for events with no initial-state radiation in the $x_{||}$ bin centered at $x_{||i}$ ($x_{||}$ is calculated relative to the true jet axis), ϵ_v is the correction for loss of events due to requiring the vertex to lie within the interaction region fiducial volume, b is the correction for background from beam-gas interactions, and δ is the radiative-correction factor as described in Eqs. (4.6), (4.7), and (4.9) of I. Initial-state radiation was included in the produced events so that the efficiency of the detector for events in a moving center-of-mass system at energy lower than $E_{\text{c.m.}}$ was included. The effects of the inclusion of initial-state radiation are an overall decrease in efficiency because nonradiative events have higher multiplicities than those in which there was significant radiation and an additional decrease in inclusive distribution efficiency for high-momentum particles because events with significant radiation cannot have particles with momentum near the beam energy. Incorrect jet-axis determination is corrected for by the shifting of particles between the produced and detected $x_{||}$ bins. It is important to include the effect of the jet-axis correction in events with significant initial-state radiation because these events do not fit the assumption of back-to-back jets. The inclusive distributions were corrected so as to include multihadronic events with all produced multiplicities, including events with two charged particles. Heavy-lepton production was not subtracted. Since only events with at

least three charged tracks were used, the effect of heavy leptons was negligible.

The corrected $s\,d\sigma/dx_{||}$ distributions versus $x_{||}$ are shown in Fig. 16. If we compare the distributions in $s\,d\sigma/dx_{||}$ with those in $s\,d\sigma/dx$ [see Fig. 17(a) of I], we see that as $E_{\text{c.m.}}$ increases the two distributions become more alike because $p_\perp$ is a decreasing fraction of p. At the lower energies the distributions have quite different shapes. When e^+e^- quark fragmentation distributions are compared, for example, with leptoproduction, they should be compared in terms of the variable $x_{||}$. Except for the $E_{\text{c.m.}}=3.0$-GeV data, the $s\,d\sigma/dx_{||}$ distributions scale for $x_{||}\gtrsim 0.1$ to within $\pm 10\%$ which is at the level of our normalization and systematic uncertainties. In order better to illustrate the scaling behavior in $x_{||}$, we show in Fig. 17 the values of $s\,d\sigma/dx_{||}$ in various $x_{||}$ bins versus $E_{\text{c.m.}}$. For $E_{\text{c.m.}}\geq 4.8$ GeV $s\,d\sigma/dx_{||}$ distributions appear to scale better than $s\,d\sigma/dx$ distributions.

In order to measure the inclusive distributions in $p_\perp$ and rapidity we found that we needed to require that a fairly high-momentum particle be detected in order to be able to find an observed jet axis which was close enough to the true jet direction that we could use the jet-model Monte Carlo simulation to calculate corrections. However, requiring that a high-momentum particle be detected biases

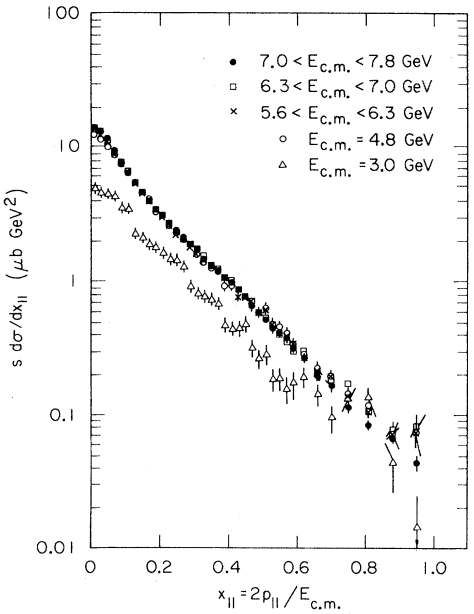

FIG. 16. Corrected single-particle inclusive $x_{||}$ distributions $s\,d\sigma/dx_{||}$ vs $x_{||}$ for various $E_{\text{c.m.}}$. $x_{||}=2p_{||}/E_{\text{c.m.}}$, where $p_{||}$ is the component of particle momentum parallel to the jet direction.

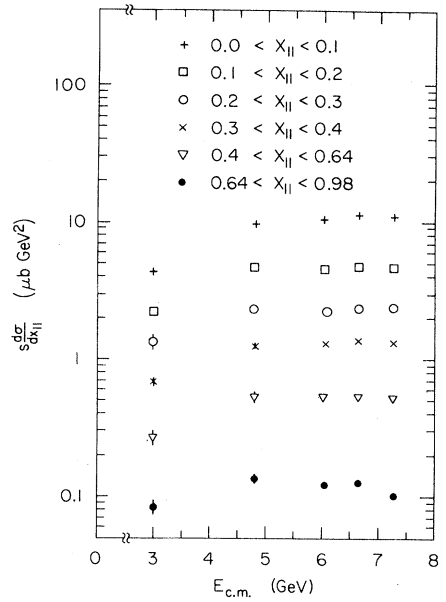

FIG. 17. Corrected single-particle inclusive $x_{||}$ distributions $s\,d\sigma/dx_{||}$ vs $E_{\text{c.m.}}$ for various $x_{||}$ ranges.

the inclusive distributions. The method used to remove the bias is the following[19]:

(1) Find the observed jet axis as described in Sec. II.

(2) Divide the event into two jets with a plane through the interaction vertex and perpendicular to the jet axis.

(3) If the highest-momentum particle on one side of the plane (x_{max}) has x greater than some minimum value, measure the inclusive distributions in $x_{||}$, $p_\perp$, and rapidity for all the particles on the *other* side of the plane from the chosen particle.

(4) Repeat step 3 for the other side of the plane. This means that an event may be counted twice in the inclusive distributions, but no particle is counted more than once. The inclusive distributions are normalized to the total number of *jets* contributing.

Corrections were calculated by applying this procedure to both the produced and detected events in the Monte Carlo simulation. For the produced events the true jet direction is known, so corrections for finding the wrong jet axis in the detected events could be calculated. The corrections, of course, are somewhat model dependent. We have some confidence in this correction procedure, however, because the jet-model distributions agree rather well with the data.

As a test of the effectiveness of this method for

removing biases due to requiring a high-momentum particle, we apply it to the $x_{||}$ distributions which we have already measured for all events. We used the highest-energy data sample, $7.0 < E_{\text{c.m.}} < 7.8$ GeV, because it has the best statistics (and also because it has the best defined jet structure).

The particle-density distribution $(1/\sigma)d\sigma/dx_{||}$ is given for each $x_{||}$ bin by

$$\frac{1}{\sigma}\frac{d\sigma}{dx_{||}}(x_{||i}) = \frac{N(x_{||i})}{\epsilon(x_{||i})(N_j/\epsilon_j)\delta x_{||i}} , \tag{4.4}$$

where $N(x_{||i})$ is the number of detected tracks in the bin centered on $x_{||} = x_{||i}$ in a jet opposite a jet containing a particle with x larger than some cut, $\epsilon(x_{||i})$ is the single-particle inclusive detection efficiency, N_j is the number of jets with $x_{\max}$ larger than the cut, ϵ_j is the efficiency for detecting such a jet, and $\delta x_{||i}$ is the bin width. Here $\epsilon(x_{||i})$ is given by

$$\epsilon(x_{||i}) = \frac{N_D(x_{||i})}{N_P(x_{||i})} , \tag{4.5}$$

where $N_D(x_{||i})$ is the number of detected particles in the $x_{||}$ bin centered at $x_{||i}$ in a jet opposite a jet containing a particle with x larger than the cut in the Monte Carlo calculation and $N_P(x_{||i})$ is the same quantity for produced events in the Monte Carlo calculation. The inclusive distributions are radiatively corrected in the same manner as for $s\,d\sigma/dx_{||}$, that is, $N_P(x_{||})$ is calculated from the produced $x_{||}$ distribution for events with no initial-state radiation. The extra correction factors in Eq. (4.3) are no longer needed since they cancel with the same quantities for the jet efficiency. ϵ_j is given by

$$\epsilon_j = \frac{N_{jD}}{N_{jP}} , \tag{4.6}$$

where N_{jD} is the number of detected jets with $x_{\max}$ larger than the cut in the Monte Carlo calculation and N_{jP} is the number of produced jets with $x_{\max}$ larger than the cut in events with no initial-state radiation.

In Fig. 18 are shown the corrected distributions $(1/\sigma)d\sigma/dx_{||}$ versus $x_{||}$ for various cuts on $x_{\max}$ (which is at positive $x_{||}$ and is not plotted) for $7.0 < E_{\text{c.m.}} < 7.8$ GeV. σ is the cross section for jets with $x_{\max}$ within the specified range and the distributions $(1/\sigma)d\sigma/dx_{||}$ are thus distributions of particle density in $x_{||}$. We see that these distributions are nearly independent of the $x_{\max}$ cut and agree with the distribution for all events for negative $x_{||}$. Only for $x_{\max} > 0.7$ do we see a significant effect in the $x_{||}$ distribution on the opposite side: requiring a particle with $x_{\max} > 0.7$ reduces the particle density for small $|x_{||}|$ and increases the particle density for large $|x_{||}|$. On the same side as the $x_{\max}$ particle we do see a correlation: the particle density decreases as $x_{\max}$ increases. We conclude that this method produces a relatively bias-free $x_{||}$ distribution for negative $x_{||}$ since the $x_{||}$ distribution opposite a jet with $x_{\max} > 0.3$ looks like the $x_{||}$ distribution for all events. The ratio of observed jets with $x_{\max} > 0.3$ to all events is 0.60 for $7.0 < E_{\text{c.m.}} < 7.8$ GeV. We chose to use $x_{\max} > 0.3$ for our analysis because the statistics are better than for the other cuts. Of those observed jets with $x_{\max} > 0.3$, only 4.7% have $x_{\max} > 0.7$, so the difference in distributions for $x_{\max} > 0.7$ has little effect on the total sample.

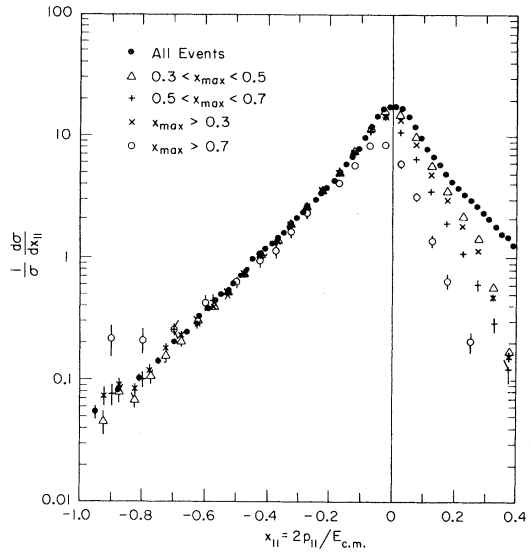

FIG. 18. Corrected particle-density distributions $(1/\sigma)d\sigma/dx_{||}$ vs $x_{||}$ for various $x_{\max}$ cuts for $7.0 < E_{\text{c.m.}} < 7.8$ GeV. $x_{\max}$ is the highest-x particle on one side of the event and is not plotted. The jet direction is oriented so that $x_{\max}$ is at positive $x_{||}$. The distributions are normalized to the cross sections for jets with $x_{\max}$ within the specified range.

In fact, we have made a physical observation: we have shown that the particle-density distribution in $x_{||}$ in one jet is independent of the $x_{\max}$ cut in the other jet. There is no particular reason why this has to be so, although it is expected in the quark-parton model. In Fig. 19 we show the $(1/\sigma)d\sigma/dx_{||}$ distributions produced by the limited-transverse-momentum jet-model Monte Carlo calculation. In contrast with the data, the Monte Carlo simulation does show a dependence of

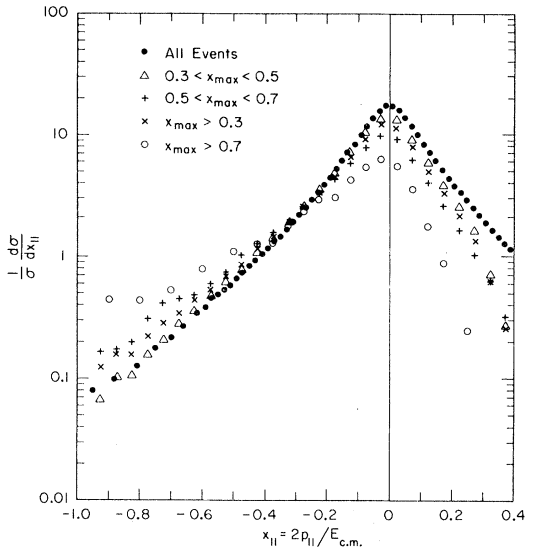

FIG. 19. Particle-density distributions $(1/\sigma)d\sigma/dx_{||}$ vs $x_{||}$ for various $x_{\max}$ cuts for jet-model Monte Carlo simulation at $E_{\text{c.m.}}=7.3$ GeV.

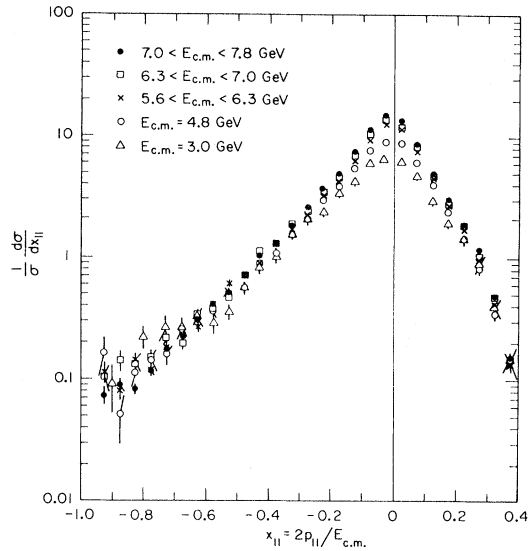

FIG. 20. Corrected particle-density distributions $(1/\sigma)d\sigma/dx_{||}$ vs $x_{||}$ for $x_{\max}>0.3$ for various $E_{\text{c.m.}}$. $x_{\max}$ is at positive $x_{||}$ and is not plotted. The distributions are normalized to the cross sections for jets with $x_{\max}>0.3$.

the negative $x_{||}$ distribution on the $x_{\max}$ cut used on the opposite side. For the Monte Carlo simulation the particle density for small $|x_{||}|$ decreases and that for large $|x_{||}|$ increases as $x_{\max}$ increases. The $x_{||}$ distribution opposite a jet with $x_{\max}>0.3$ is significantly different from the distribution for all events.

The corrected $(1/\sigma)d\sigma/dx_{||}$ distributions for $x_{\max}>0.3$ for the data at various $E_{\text{c.m.}}$ are shown in Fig. 20. $(1/\sigma)d\sigma/dx_{||}$ distributions for all events at the same energies are shown in Fig. 21, where σ is the event cross section. The distributions in Fig. 20 for negative $x_{||}$ agree quite well with those in Fig. 21 for all $x_{||}$ considered to be positive if those in Fig. 21 are divided by two (because the distributions in Fig. 21 are for both jets). We see that the method works well for all energies, that is, the $x_{||}$ distributions opposite a jet with $x_{\max}>0.3$ look like those for all events. To obtain $(1/\sigma)d\sigma/dx_{||}$ for all events from $(1/\sigma)d\sigma/dx_{||}$ for particles opposite a jet with $x_{\max}>0.3$, assume that the distribution for positive $x_{||}$ is the reflection of that for negative $x_{||}$ about $x_{||}=0$. One observation that can be made about the distributions $(1/\sigma)d\sigma/dx_{||}$ for the various energies is that they scale rather well for all energies, including 3.0 GeV, for $x_{||}\geq 0.2$. That $(1/\sigma)d\sigma/dx_{||}$ scales for $E_{\text{c.m.}}\geq 4.8$ GeV is not surprising since $s\,d\sigma/dx_{||}$ scales and R is approximately constant. However, R at 3.0 GeV is a factor of 1.6 smaller than R at the higher energies. Evidently, normalizing the inclusive distributions in $x_{||}$ to the total hadronic

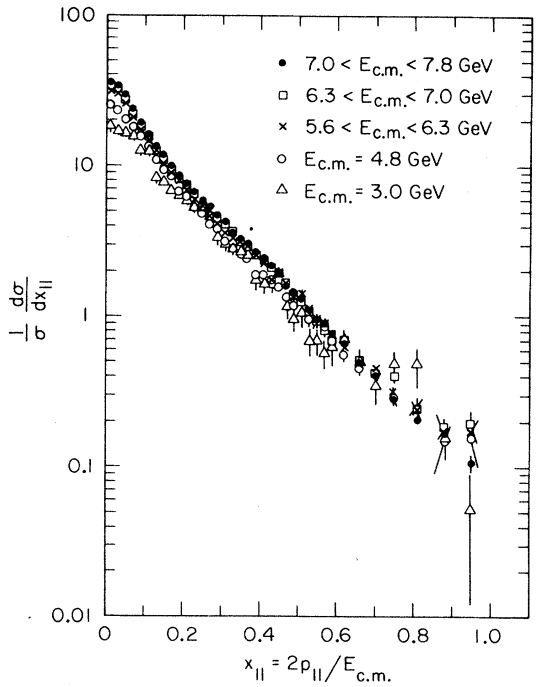

FIG. 21. Corrected particle-density distributions $(1/\sigma)d\sigma/dx_{||}$ vs $x_{||}$ for all events for various $E_{\text{c.m.}}$. The distributions are normalized to the total cross sections for multihadronic events.

cross section rather than the integrated luminosity makes up for this difference.

Inclusive distributions in rapidity and $p_\perp$ relative to the jet direction were then measured using the method just described. The rapidity y is defined by

$$y=\tfrac{1}{2}\ln\left[\frac{E+p_{||}}{E-p_{||}}\right], \tag{4.7}$$

where E is the energy of the particle assuming a pion mass. Figure 22 shows the corrected particle-density distributions $(1/\sigma)d\sigma/dy$ versus y for various $x_{\max}$ cuts for $7.0<E_{\text{c.m.}}<7.8$ GeV. As was the case for $(1/\sigma)d\sigma/dx_{||}$ for negative $x_{||}$, we see that the distributions for negative y are nearly independent of the $x_{\max}$ cut. For $x_{\max}>0.7$ there is a decrease in particle density for y between -1.5 and 0. For positive y, of course, we see a decrease in multiplicity as the $x_{\max}$ cut increases, as was noted previously for the $x_{||}$ distributions. We then used the cut $x_{\max}>0.3$ to produce corrected distributions in rapidity density at the other energies, as shown in Fig. 23. The unbiased distributions of particles in rapidity relative to the jet direction would look like Fig. 23 with the distributions for positive y given by reflections of those for negative y about $y=0$. Or, equivalently, the distributions for negative y multiplied by two could be plotted as $(1/\sigma)d\sigma/d\,|y|$ versus $|y|$ in order to compare with conventional presentations. The distributions $(1/\sigma)d\sigma/dy$ increase in width as $E_{\text{c.m.}}$ increases. The distributions for the three highest energy ranges are quite similar in shape and appear to level off to a plateau for y between -1.0 and 0. The value of $(1/\sigma)d\sigma/dy$ at the plateau is about 1.45 and is somewhat energy dependent. The dip in $(1/\sigma)d\sigma/dy$ for y between -0.2 and 0 may be due to systematic errors in our data analysis. Because of tracking problems, we did not use particles with transverse momentum relative to the beam direction less than 150 MeV/c and were required to rely on the Monte Carlo simulation to correct for this cut.

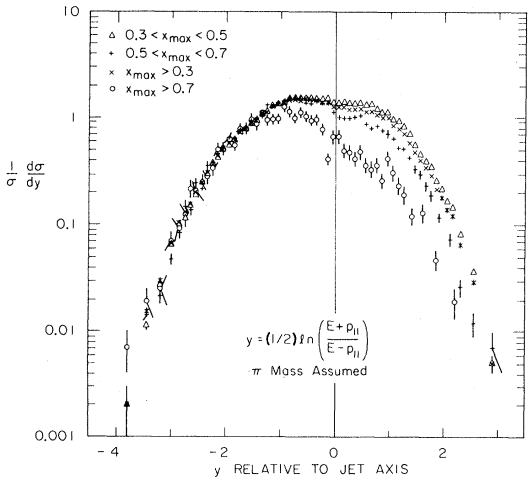

FIG. 22. Corrected particle-density distributions $(1/\sigma)d\sigma/dy$ vs y for various $x_{\max}$ cuts for $7.0<E_{\text{c.m.}}<7.8$ GeV. $x_{\max}$ is the highest-x particle on one side of the event and is not plotted. The jet direction is oriented so that $x_{\max}$ is at positive y. The distributions are normalized to the cross sections for jets with $x_{\max}$ within the specified range.

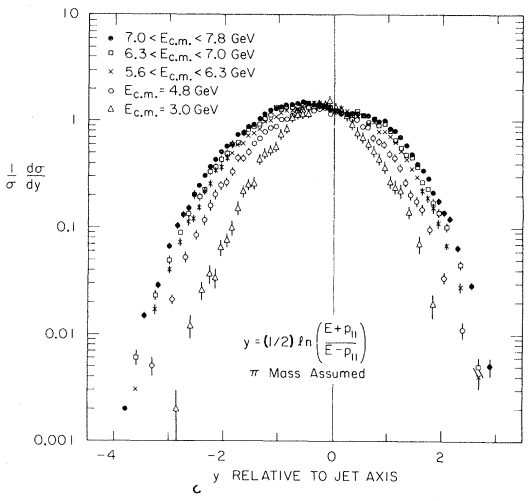

FIG. 23. Corrected particle-density distributions $(1/\sigma)d\sigma/dy$ vs y for $x_{\max}>0.3$ for various $E_{\text{c.m.}}$. y is the rapidity of the particle relative to the jet direction assuming a pion mass. $x_{\max}$ is at positive y and is not plotted. The distributions are normalized to the cross sections for jets with $x_{\max}>0.3$.

Inclusive distributions in $p_\perp$ relative to the jet direction are of considerable interest because they are the basis of the definition of jet structure. Figure 24 shows the corrected distributions $(1/\sigma)d\sigma/dp_\perp{}^2$ versus $p_\perp{}^2$ for particles opposite (negative $x_{||}$) jets with various $x_{\max}$ cuts for $7.0<E_{\text{c.m.}}<7.8$ GeV. The distributions are independent of the $x_{\max}$ cut, except for $x_{\max}>0.7$ which shows a decrease in particle density for $p_\perp{}^2<0.6$ (GeV/c)^2. The corrected distributions $(1/\sigma)d\sigma/dp_\perp{}^2$ versus $p_\perp{}^2$ measured for particles opposite jets with $x_{\max}>0.3$ for the various $E_{\text{c.m.}}$ values are presented in Fig. 25. The $p_\perp{}^2$ distributions are very similar in shape for $E_{\text{c.m.}}\geq 4.8$ GeV. The area under each curve increases as $E_{\text{c.m.}}$ increases because of the increasing multiplicity. For $E_{\text{c.m.}}=3.0$ GeV the $p_\perp{}^2$ distribution falls off slight-

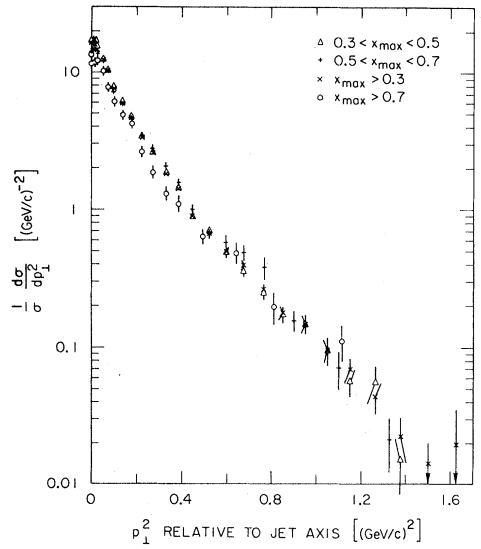

FIG. 24. Corrected $(1/\sigma)d\sigma/dp_\perp{}^2$ vs $p_\perp{}^2$ for particles opposite jets with various $x_{\max}$ cuts for $7.0 < E_{\text{c.m.}} < 7.8$ GeV. $p_\perp$ is the component of particle momentum perpendicular to the jet direction. The distributions are normalized to the cross sections for jets with $x_{\max}$ within the specified range.

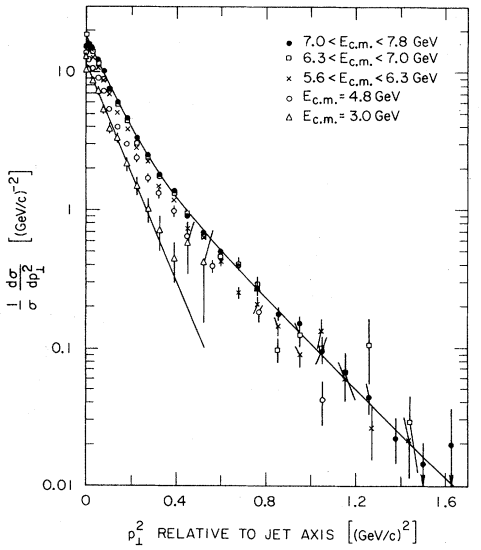

FIG. 25. Corrected $(1/\sigma)d\sigma/dp_\perp{}^2$ vs $p_\perp{}^2$ for particles opposite (negative $x_{||}$) jets with $x_{\max} > 0.3$ for various $E_{\text{c.m.}}$. $p_\perp$ is the component of particle momentum perpendicular to the jet direction. The distributions are normalized to the cross sections for jets with $x_{\max} > 0.3$. The solid lines represent the fits, discussed in the text, to the distributions for $E_{\text{c.m.}} = 3.0$ GeV and $7.0 < E_{\text{c.m.}} < 7.8$ GeV.

ly faster as $p_\perp{}^2$ increases and there are no particles with $p_\perp{}^2 > 0.6$ (GeV/c)^2. The values of the differential cross sections in the distributions shown in Fig. 25 should be multiplied by two since they represent only one of the two jets in an event.

In order to illustrate how the corrections might affect the $p_\perp{}^2$ distributions we present in Fig. 26 the uncorrected observed distributions $(1/N_{\text{ev}})dN/dp_\perp{}^2$ for particles opposite jets with $x_{\max} > 0.3$, where N_{ev} is the number of observed jets with $x_{\max} > 0.3$ and $dN/dp_\perp{}^2$ is the number of particles observed per (GeV/c)^2 in each $p_\perp{}^2$ bin. By comparing Figs. 25 and 26 one can see that the effect of the Monte Carlo corrections is to increase the particle density at high $p_\perp{}^2$ relative to that at low $p_\perp{}^2$. This is because the detector acceptance makes it more difficult to detect both a jet and a particle at high $p_\perp$ to it. In any case, the Monte Carlo corrections do not change appreciably the similarity in shapes of the distributions for $E_{\text{c.m.}} \geq 4.8$ GeV nor do they change the observation that the slopes decrease as $p_\perp{}^2$ increases.

Figure 27 shows the same distributions as in Fig. 25 plotted versus $p_\perp$ rather than $p_\perp{}^2$. These distributions were used to calculate the average transverse momentum relative to the jet direction $\langle p_\perp \rangle$ for each of the $E_{\text{c.m.}}$. Figure 28 shows $\langle p_\perp \rangle$ oppo-

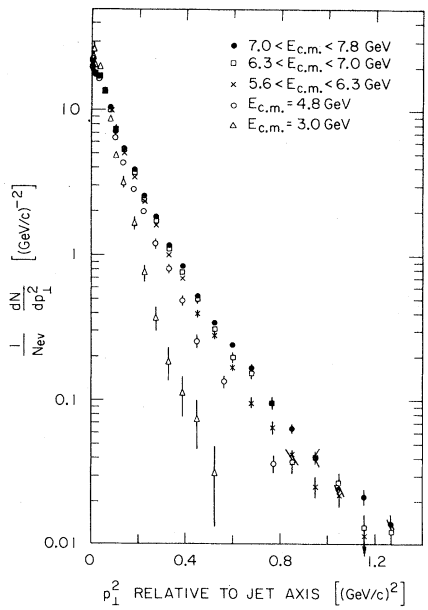

FIG. 26. Observed $(1/N_{\text{ev}})\ dN/dp_\perp{}^2$ for particles opposite jets with $x_{\max} > 0.3$ in events with three or more charged particles. N_{ev} is the number of observed jets with $x_{\max} > 0.3$ and $dN/dp_\perp{}^2$ is the number of particles observed per (GeV/c)^2 in each $p_\perp{}^2$ bin.

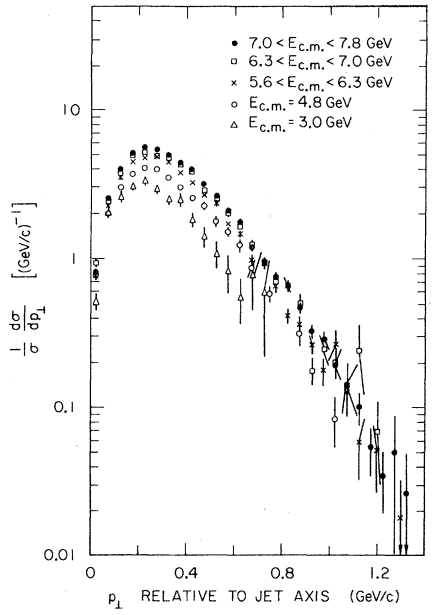

FIG. 27. Corrected $(1/\sigma)d\sigma/dp_\perp$ vs $p_\perp$ for particles opposite jets with $x_{\max}>0.3$ for various $E_{\text{c.m.}}$. $p_\perp$ is the component of particle momentum perpendicular to the jet direction. The distributions are normalized to the cross sections for jets with $x_{\max}>0.3$.

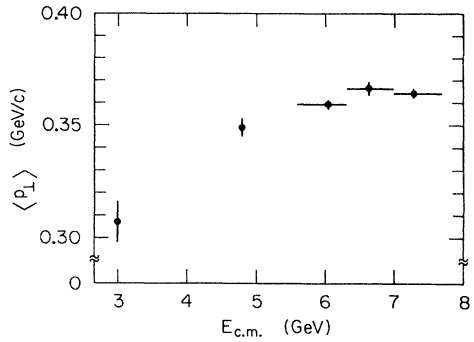

FIG. 28. Average transverse momentum relative to the jet direction $\langle p_\perp\rangle$ for particles opposite jets with $x_{\max}>0.3$ vs $E_{\text{c.m.}}$.

site jets with $x_{\max}>0.3$ versus $E_{\text{c.m.}}$. The dependence of $\langle p_\perp\rangle$ on $E_{\text{c.m.}}$ is simple evidence for jet structure since $\langle p_\perp\rangle$ levels off as $E_{\text{c.m.}}$ increases. The value of $\langle p_\perp\rangle$ for $7.0<E_{\text{c.m.}}<7.8$ GeV is 364 ± 2 MeV/c where the error is statistical only. To estimate the systematic error we calculated $\langle p_\perp\rangle$ for various $x_{\max}$ cuts for $7.0<E_{\text{c.m.}}<7.8$ GeV (see Fig. 24 for $p_\perp{}^2$ distributions for these $x_{\max}$ cuts). The range of $\langle p_\perp\rangle$ for different $x_{\max}$ cuts was within ±10 MeV/c of $\langle p_\perp\rangle$ for $x_{\max}>0.3$, so we estimate the systematic error for $\langle p_\perp\rangle$ to be ±10 MeV/c.

The distributions $(1/\sigma)d\sigma/dp_\perp{}^2$ versus $p_\perp{}^2$, shown in Fig. 25, do not fit single exponentials in $p_\perp{}^2$, as might have been expected from phenomenological arguments, except at $E_{\text{c.m.}}=3.0$ GeV. For $E_{\text{c.m.}}\geq4.8$ GeV the $p_\perp{}^2$ distributions fit reasonably well to a sum of two exponentials in $p_\perp{}^2$: $(1/\sigma)d\sigma/dp_\perp{}^2=c_1e^{-b_1p_\perp^2}+c_2e^{-b_2p_\perp{}^2}$; the parameters for such fits are given in Table I. Only statistical errors were used to determine χ^2. The distributions given by the single exponential fit for $E_{\text{c.m.}}=3.0$ GeV and by the sum-of-two-exponentials fit for $7.0<E_{\text{c.m.}}<7.8$ GeV are represented by the solid lines in Fig. 25. The coefficients of $p_\perp{}^2$, b_1 and b_2, are plotted versus $E_{\text{c.m.}}$ in Figs. 29(a) and 29(b). The larger coefficient b_1 is consistent with about 10 $(\text{GeV}/c)^{-2}$ for the three highest energy ranges; it is a little larger at 4.8 GeV and a little smaller at 3.0 GeV. The smaller coefficient b_2 is consistent with about 4 $(\text{GeV}/c)^{-2}$ for all energies $E_{\text{c.m.}}\geq4.8$ GeV. Thus we have shown quantitatively that the shapes of the $p_\perp{}^2$ distributions are quite similar for $E_{\text{c.m.}}\geq4.8$ GeV.

In Fig. 30 we compare the $p_\perp{}^2$ distribution for $7.0<E_{\text{c.m.}}<7.8$ GeV with that for the jet-model Monte Carlo simulation. We see that for $p_\perp{}^2>0.6$ $(\text{GeV}/c)^2$ the Monte Carlo distribution is lower than the data. $\langle p_\perp\rangle$ for the Monte Carlo distribution is 343 MeV/c, about 20 MeV/c lower than for the data. We also note that the Monte Carlo distribution is not a single exponential in $p_\perp{}^2$. What

TABLE I. Fits to $(1/\sigma)d\sigma/dp_\perp{}^2=c_1e^{-b_1p_\perp{}^2}+c_2e^{-b_2p_\perp{}^2}$ for particles opposite jets with $x_{\max}>0.3$ for various $E_{\text{c.m.}}$ for $p_\perp{}^2>0.01$ $(\text{GeV}/c)^2$.

$E_{\text{c.m.}}$ (GeV)	c_1 $[(\text{GeV}/c)^{-2}]$	b_1 $[(\text{GeV}/c)^{-2}]$	c_2 $[(\text{GeV}/c)^{-2}]$	b_2 $[(\text{GeV}/c)^{-2}]$	χ^2	Degrees of freedom
3.0	11.08±0.45	8.95±0.42			10.40	11
4.8	9.37±0.86	13.18±1.56	4.93±0.98	4.43±0.36	4.86	11
5.6–6.3	12.15±0.69	10.41±0.68	4.13±0.80	3.93±0.27	23.75	19
6.3–7.0	11.53±1.01	11.07±1.08	5.87±1.17	4.25±0.30	36.70	18
7.0–7.8	13.97±0.49	10.23±0.44	4.62±0.56	3.77±0.17	29.86	21

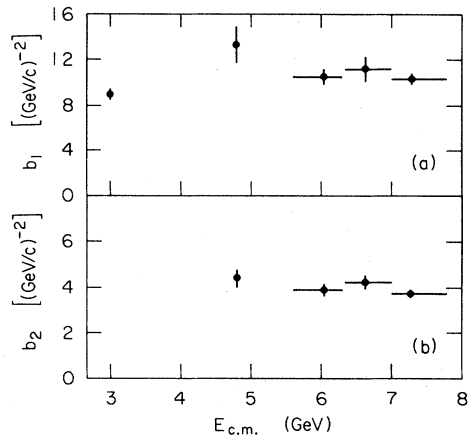

FIG. 29. Coefficients of $p_\perp{}^2$, (a) b_1 and (b) b_2, for fits of the form $(1/\sigma)d\sigma/dp_\perp{}^2 = c_1 e^{-b_1 p_\perp{}^2} + c_2 e^{-b_2 p_\perp{}^2}$ for particles opposite jets with $x_{max} > 0.3$ vs $E_{c.m.}$.

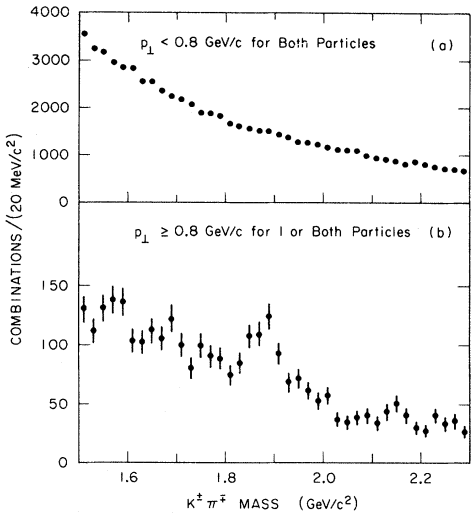

FIG. 31. $K^\pm\pi^\mp$ invariant-mass distributions for $7.0 < E_{c.m.} < 7.8$ GeV for (a) both particles with $p_\perp < 0.8$ GeV/c and (b) one or both particles with $p_\perp \geq 0.8$ GeV/c. $p_\perp$ is the component of particle momentum perpendicular to the observed jet axis. No time-of-flight information was used; each combination was plotted twice—once for each mass assignment.

could be the reason for the excess of high-$p_\perp$ particles? The answer may be found in Figs. 31(a) and 31(b) which show the $K^\pm\pi^\mp$ invariant-mass distributions for $7.0 < E_{c.m.} < 7.8$ GeV for both particles with $p_\perp < 0.8$ GeV/c and for one or both particles with $p_\perp \geq 0.8$ GeV/c. (No time-of-flight information was used; each combination was plotted twice—once for each mass assignment.) For the first case we see no signal, but for the second case we see a peak near the D^0 mass of 1864 MeV/c^2.[20] We therefore have conclusive evidence that some

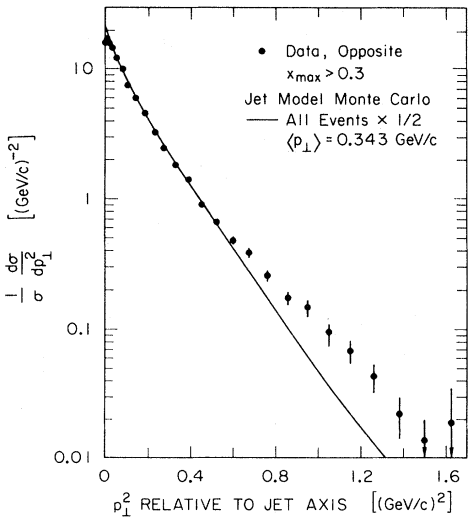

FIG. 30. Comparison of the corrected $(1/\sigma)d\sigma/dp_\perp{}^2$ vs $p_\perp{}^2$ for particles opposite jets with $x_{max} > 0.3$ for $7.0 < E_{c.m.} < 7.8$ GeV with the produced jet-model Monte Carlo distribution for all events at $E_{c.m.} = 7.3$ GeV.

of the high-$p_\perp$ particles are the result of D^0 production and decay into $K^-\pi^+$. Other D decays have been studied by Monte Carlo, but only the two-body decay $D^0 \to K^-\pi^+$ contributes significantly to the $p_\perp > 0.8$ GeV/c region. In fact, it is possible, although this hypothesis should not be taken quantitatively, to produce a quite adequate representation of the observed $p_\perp{}^2$ distribution by adding to the jet-model Monte Carlo simulation a contribution from phase-space production of $D^0\bar{D}^0{}^*\pi^+\pi^-$, where $D^{0*} \to D^0\gamma$ or $D^0\pi^0$ and D^0 decays only to $K^-\pi^+$, as shown in Fig. 32. The relative normalization of the two models was chosen by requiring that the number of high-$p_\perp{}^2$ particles agree with the data. One should note that all high-$p_\perp$ particles do not necessarily come from charmed-particle decays, and we cannot show that the second exponential in $p_\perp{}^2$ is completely due to charm. Some high-$p_\perp$ particles can result from ordinary two-jet production, and the jet-model $p_\perp{}^2$ distribution is not a single exponential in $p_\perp{}^2$.

We have measured the dependence of the $p_\perp$ distributions on $x_{||}$, or Feynman x, for $7.0 < E_{c.m.} < 7.8$ GeV. Figure 33 shows the corrected distributions $(1/\sigma)d\sigma/dp_\perp{}^2$ versus $p_\perp{}^2$ for several $x_{||}$ ranges for particles opposite jets with $x_{max} > 0.3$. The distributions are normalized to the cross section for jets with $x_{max} > 0.3$. From these distribu-

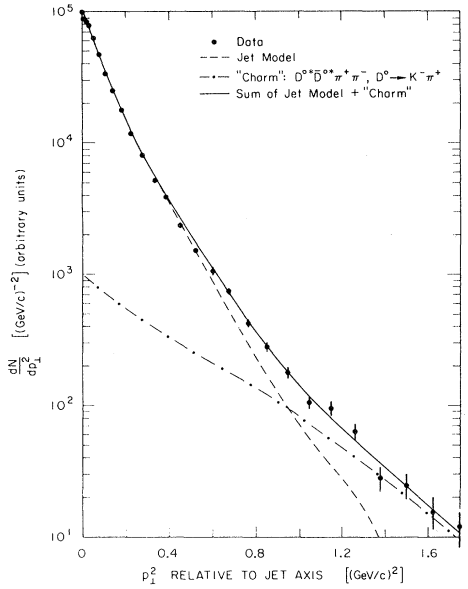

FIG. 32. Observed $p_\perp{}^2$ distribution for particles opposite jets with $x_{\max} > 0.3$ in events with three or more charged particles for $7.0 < E_{\text{c.m.}} < 7.8$ GeV. $p_\perp$ is the component of particle momentum perpendicular to the observed jet axis. The data is compared with the sum of the Monte Carlo predictons of the jet model and a charmed meson production model. The Monte Carlo distribution is normalized to the total number of particles in the data. The relative normalization of the two models was chosen by requiring that the number of high-$p_\perp{}^2$ particles agree with the data.

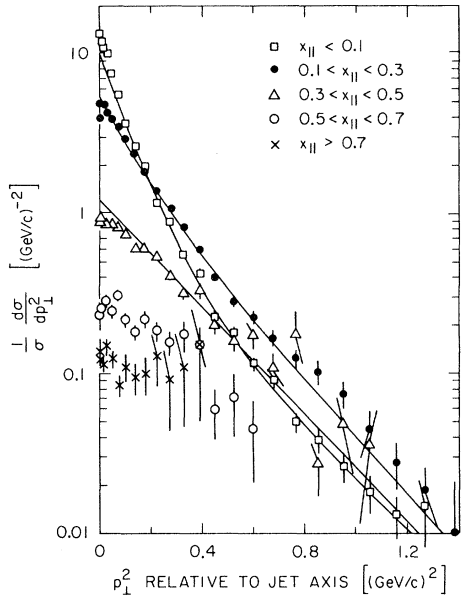

FIG. 33. Corrected $(1/\sigma)d\sigma/dp_\perp{}^2$ for particles in various $x_{||}$ ranges opposite jets with $x_{\max} > 0.3$ for $7.0 < E_{\text{c.m.}} < 7.8$ GeV. The distributions are normalized to the cross section for jets with $x_{\max} > 0.3$. The solid lines represent the fits discussed in the text.

tions we see that particles with $x_{||}$ between 0.1 and 0.3 are the major contributors to the high-$p_\perp{}^2$ region. Particles with $x_{||}$ less than 0.1 and between 0.3 and 0.5 contribute about equally to the high-$p_\perp{}^2$ region. We were able to calculate $\langle p_\perp \rangle$ for the $x_{||}$ ranges with $x_{||}$ less than 0.5; the $p_\perp$ distributions for $x_{||}$ greater than 0.5 are too poorly defined because of the limited statistics to allow a calculation of $\langle p_\perp \rangle$. In Fig. 34 we present $\langle p_\perp \rangle$ versus $x_{||}$ for three $x_{||}$ ranges. $\langle p_\perp \rangle$ increases with increasing $x_{||}$ in a manner quite like the "seagull" effect seen in hadronic physics and leptoproduction.[21]

The $p_\perp{}^2$ distributions for $x_{||} < 0.1$ and $0.1 < x_{||} < 0.3$ can be fitted to sums of two exponentials in $p_\perp{}^2$, while the distribution for $0.3 < x_{||} < 0.5$ requires only a single exponential. The parameters of the fits to $(1/\sigma)d\sigma/dp_\perp{}^2 = c_1 e^{-b_1 p_\perp{}^2} + c_2 e^{-b_2 p_\perp{}^2}$ are listed in Table II. The minimum $p_\perp{}^2$ used in the fits was varied somewhat to obtain reasonable fits. The fitted distributions are represented by the solid lines in Fig. 33. The values of the coefficients of $p_\perp{}^2$, b_1 and b_2, are plotted versus $x_{||}$ in Figs. 35(a) and 35(b). Since the single coefficient for $0.3 < x_{||} < 0.5$ was in agreement with the smaller coefficient for the other two $x_{||}$ ranges, it was plotted in Fig. 35(b). The large coefficients for $x_{||} < 0.1$ and $0.1 < x_{||} < 0.3$ are both consistent with 10 $(\text{GeV}/c)^{-2}$, the same value that was found for the $p_\perp{}^2$ distribution integrated over $x_{||}$. The smaller coefficients and the single coefficient for $0.3 < x_{||} < 0.5$ are consistent with 4 $(\text{GeV}/c)^{-2}$, again in agreement with the smaller

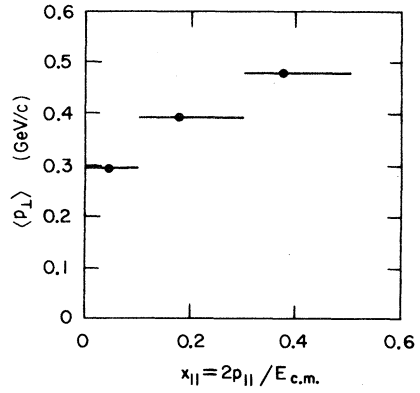

FIG. 34. Average transverse momentum relative to the jet direction $\langle p_\perp \rangle$ vs $x_{||}$ for particles opposite jets with $x_{\max} > 0.3$ for $7.0 < E_{\text{c.m.}} < 7.8$ GeV.

TABLE II. Fits to $(1/\sigma)d\sigma/dp_\perp{}^2=c_1e^{-b_1p_\perp{}^2}+c_2e^{-b_2p_\perp{}^2}$ for particles in various $x_{||}$ ranges opposite jets with $x_{\max}>0.3$ for $7.0<E_{\text{c.m.}}<7.8$ GeV.

$x_{||}$ range	c_1 [(GeV/c)$^{-2}$]	b_1 [(GeV/c)$^{-2}$]	c_2 [(GeV/c)$^{-2}$]	b_2 [(GeV/c)$^{-2}$]	χ^2	Degrees of freedom
<0.1 $p_\perp{}^2>0.09$ (GeV/c)^2	8.98±0.47	10.37±0.72	0.96±0.33	3.79±0.41	19.17	15
0.1–0.3 $p_\perp{}^2>0.04$ (GeV/c)^2	3.09±0.47	8.82±1.12	2.50±0.52	4.17±0.24	21.44	17
0.3–0.5 $p_\perp{}^2>0.16$ (GeV/c)^2	1.24±0.09	3.88±0.21			15.69	11

coefficient for the $p_\perp{}^2$ distribution integrated over $x_{||}$. If we were to assume that the exponential with the smaller slope is due to charmed-particle production, then we would be forced to conclude that all particles with $0.3<x_{||}<0.5$ are the result of charmed-particle decay, which is unlikely. Unfortunately, we have been able to study only the decay $D^0\to K^-\pi^+$ which has a branching ratio of only $(3.0\pm0.6)\%$.[20] We have been otherwise unable to separate the charm production component in this analysis.

We have looked for charge correlations between the leading particle in one jet and all other observed particles in events with three or more detected charged particles. The data sample used was the highest energy range $7.0<E_{\text{c.m.}}<7.8$ GeV. We plotted $x_{||}$ distributions using the same method as was described in connection with Fig. 18, except that two distributions were produced—one for those particles with the same charge as $x_{\max}$ and another for those particles with the opposite charge to the $x_{\max}$ particle. In Fig. 36 we present the observed ratio (opposite charge)/(same charge) of these two distributions in $x_{||}$ for two different $x_{\max}$ cuts: $x_{\max}>0.5$ and $x_{\max}>0.7$. $x_{\max}$ is at positive $x_{||}$, and, of course, is not included. For these distributions we have used only events in which the total charge was 0 if an even number of particles was observed or ±1 if an odd number was observed. In general, since the detector did not have complete acceptance, one or more particles were not detected, so we do not expect to conserve charge. Given the charged-particle multiplicity distribution for each $x_{||}$ bin, we could calculate the statistical expectation for the charge ratio as a function of $x_{||}$. For example, for an event with three charged particles and total charge ±1 the probability that any two particles have opposite charge is $\frac{2}{3}$ and the probability that any two particles have the same charge is $\frac{1}{3}$, so the ratio of opposite charge to same charge is expected to be 2. The expected ratio decreases as the multiplicity increases. The statistical expectation versus $x_{||}$ is represented by the dashed line in Fig. 36.

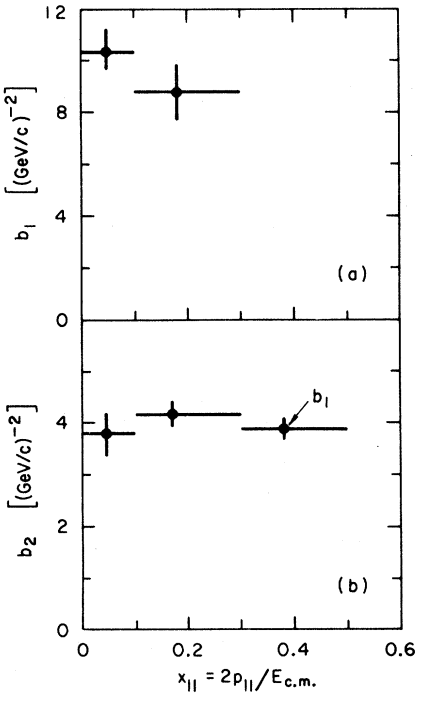

FIG. 35. Coefficients (a) b_1 and (b) b_2 for fits of the form $(1/\sigma)d\sigma/dp_\perp{}^2=c_1e^{-b_1p_\perp{}^2}+c_2e^{-b_2p_\perp{}^2}$ vs $x_{||}$ for particles opposite jets with $x_{\max}>0.3$ for $7.0<E_{\text{c.m.}}<7.8$ GeV.

We see that for positive $x_{||}$ the ratio of opposite charge to same charge is much larger than the statistical expectation. This means that there are same-side correlations: particles in the same jet as the $x_{\max}$ particle tend to have the opposite charge to the $x_{\max}$ particle. Such an effect can be caused by neutral resonances and is expected for various other models. For negative $x_{||}$ there is no evidence for charge correlations. (Such correlations would be long-range charge correlations.) For $x_{\max}>0.7$

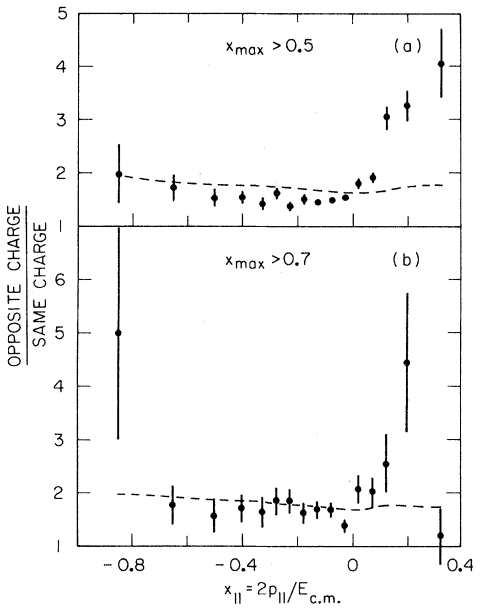

FIG. 36. Observed ratio of the number of particles with opposite charge to the x_{max} particle to the number of particles with the same charge as x_{max} for (a) $x_{max} > 0.5$ and (b) $x_{max} > 0.7$ vs $x_{||}$ for $7.0 < E_{c.m.} < 7.8$ GeV. x_{max} is at positive $x_{||}$. The statistical expectations, calculated from the charged-particle multiplicity distributions for each $x_{||}$ bin, are represented by the dashed lines.

the point at $x_{||} = -0.85$ is high compared with the statistical expectation, but the difference is not statistically significant. There were only 18 events contributing to this point. Of these 3 had the same charge as x_{max} and 15 had the opposite charge, whereas we would have expected 6 and 12. The probability of observing a charge ratio of 5 or more is about 10%.

The statistical expectation is generally a little larger than the measured charge ratio for negative $x_{||}$. In principle, when calculating the statistical expectation for negative $x_{||}$ we should have taken into account the observed charge correlation at positive $x_{||}$. This would have had the effect of lowering the statistical expectation slightly for negative $x_{||}$. The effect would be small because the number of particles at positive $x_{||}$ is small for such large x_{max} cuts (see Fig. 18). Some quark-parton models predict a charge correlation between leading particles in opposite jets due to their production from a quark-antiquark pair. Particles with $x_{||} < -0.5$ are certainly the leading particles in the jet opposite the jet with x_{max}, yet we see no such effect. It may be that to see these leading-particle charge correlations, both particles must have x very near 1; unfortunately, the statistics of our data sample, even with 52 000 events, are not sufficient for such a measurement. Also, since events with a high-x particle at this energy have low multiplicities, charge correlation due to charge conservation makes other charge correlation effects more difficult to observe.

V. CONCLUSIONS

Studies of hadron production by e^+e^- annihilation have yielded very exciting and fundamental results. Among these results is the strong evidence for jet structure for $E_{c.m.} \geq 4.8$ GeV as shown by the agreement of the observed sphericity distributions with the jet model rather than the phase-space-model predictions. By making use of the transversely polarized e^+ and e^- beams at 7.4 GeV, the jet-axis angular distribution was measured to be proportional to $1 + (0.97 \pm 0.14)\cos^2\theta$, consistent with that for a pair of spin-$\frac{1}{2}$ particles. A jet-model Monte Carlo simulation is able to reproduce not only the sphericity distributions for whole events but also the single-particle inclusive momentum and angular distributions.

Inclusive distributions in $s\,d\sigma/dx_{||}$, where $x_{||}$ = Feynman $x = 2p_{||}/E_{c.m.}$ and $p_{||}$ is the component of particle momentum parallel to the jet direction, scale for $x_{||} > 0.1$ for $E_{c.m.} \geq 4.8$ GeV to within $\pm 10\%$, which is at the level of our normalization and systematic uncertainties. Inclusive distributions in $(1/\sigma)d\sigma/dx_{||}$, where σ is the total hadronic cross section, scale rather well for $x_{||} \geq 0.2$ for all energies between 3.0 and 7.8 GeV away from the resonance regions. The $x_{||}$ distribution for one jet is nearly independent of the magnitude of the momentum of the leading particle in the other jet.

Distributions in rapidity with respect to the jet direction have been measured and show the development of a plateau for the three highest energy regions measured, from 5.6 to 7.8 GeV.

Distributions in $p_\perp{}^2$ relative to the jet direction have been measured. The average $p_\perp$ has been measured as a function of $E_{c.m.}$ and levels off at a constant value for the three highest energy regions measured, giving direct evidence for jet structure. The $p_\perp{}^2$ distributions do not agree with a simple limited-transverse-momentum jet model. The distributions in $p_\perp{}^2$ can be fitted to the sum of two exponentials in $p_\perp{}^2$. Charmed-meson production accounts for some of the high-$p_\perp$ particles observed. Distributions in $p_\perp{}^2$ as a function of $x_{||}$

have been measured for $7.0 < E_{\text{c.m.}} < 7.8$ GeV. The average $p_\perp$ increases with increasing $x_\parallel$ for $x_\parallel \leq 0.5$.

Evidence for same-side charge correlations has been found: particles in the same jet as a large-x leading particle tend to have charge opposite to that of the leading particle. There is no evidence for opposite-side charge correlations.

The data are in general agreement with the predictions of quark-parton constituent models. The recent data from PETRA[22] for e^+e^- annihilation at energies up to $E_{\text{c.m.}} = 36$ GeV have confirmed the results reported here from the Mark I detector at SPEAR and have extended the analysis to the confirmation of the QCD predictions of three- and four-jet events.

ACKNOWLEDGMENT

This work was supported by the Department of Energy under Contracts Nos. DE-AC03-76SF00515 and W-7405-ENG-48.

---

[a] Present address: Vanderbilt University, Nashville, TN 37235.
[b] Present address: General Electric, Schenectady, NY 12301.
[c] Present address: Cornell University, Ithaca, NY 14853.
[d] Present address: Laboratoire de l'Accélérateur Linéaire, Centre d'Orsay de l'Université de Paris Sud, 91405 Orsay CEDEX, France.
[e] Present address: DESY, 2000 Hamburg-52, Federal Republic of Germany.
[f] Present address: University of California, Santa Barbara, CA 93106.
[g] Present address: Business Enhancements Compuservice, Escondido, CA 92027.
[h] Present address: Hewlett Packard, Palo Alto, CA 94304.
[i] Present address: Laboratori Nazionali, 00044 Frascati, Rome, Italy.
[j] Present address: LBL, Berkeley, CA 94720.
[k] Present address: Fermilab, P.O. Box 500, Batavia, IL 60510.
[l] Present address: CERN, 1211 Geneva 23, Switzerland.
[m] Present address: Harvard University, Cambridge, MA 02138.
[n] Present address: Bell Laboratories, Naperville, IL 60566.
[o] Present address: LPNHE, Université Paris VII, 75230 Paris CEDEX 5, France.
[p] Present address: IBM Research, San Jose, CA 95123.
[q] Present address: In House Systems, New York, NY 10038.
[r] Present address: SLAC, Stanford, CA 94305.
[s] Present address: Stanford University, Stanford, CA 94305.
[t] Present address: LPNHE, Université Pierre et Marie Curie, 75230 Paris CEDEX 5, France.
[u] Present address: CEN, Saclay 91190 Gif-sur-Yvette, France.
[v] Present address: MIT, Cambridge, MA 02139.
[w] Present address: University of Illinois at Urbana-Champaign, Urbana, IL 61801.

[1] J. L. Siegrist *et al.* (preceding paper) Phys. Rev. D 26, 969 (1982).
[2] S. D. Drell, D. J. Levy, and T. M. Yan, Phys. Rev. 187, 2159 (1969); Phys. Rev. D 1, 1617 (1970).
[3] N. Cabibbo, G. Parisi, and M. Testa, Lett. Nuovo Cimento 4, 35 (1970).
[4] J. D. Bjorken and S. J. Brodsky, Phys. Rev. D 1, 1416 (1970).
[5] R. P. Feynman, *Photon-Hadron Interactions* (Benjamin, New York, 1972), p. 166.
[6] G. Hanson *et al.*, Phys. Rev. Lett. 35, 1609 (1975).
[7] J.-E. Augustin *et al.*, Phys. Rev. Lett. 33, 1406 (1974); J. J. Aubert *et al.*, *ibid.* 33, 1404 (1974); C. Bacci *et al.*, *ibid.* 33, 1408 (1974); 33, 1649 (1974); W. Braunschweig *et al.*, Phys. Lett. 53B, 393 (1974); G. S. Abrams *et al.*, Phys. Rev. Lett. 33, 1453 (1974); P. A. Rapidis *et al.*, *ibid.* 39, 526 (1977); W. Bacino *et al.*, *ibid.* 40, 671 (1978).
[8] J. Siegrist *et al.*, Phys. Rev. Lett. 36, 700 (1976); G. Goldhaber *et al.*, *ibid.* 37, 255 (1976); I. Peruzzi *et al.*, *ibid.* 37, 569 (1976).
[9] The method is based on a suggestion in a footnote in Ref. 4.
[10] G. Hanson, in *Proceedings of the Seventh International Colloquium on Multiparticle Production, Tutzing, Germany, 1976,* edited by J. Benecke *et al.*, (Max Planck Institute, Munich, Germany, 1976), p. 313; in *Proceedings of the XVIIIth International Conference on High Energy Physics, Tbilisi, 1976,* edited by N. N. Bogolubov *et al.* (JINR, Dubna, U.S.S.R., 1977), Vol. II, p. B1.
[11] The model used was GENIS, which is described in R. B. Chaffee, SLAC Computation Group Technical Memo No. 195, 1979 (unpublished). GENIS uses the technique of L. Van Hove, Nucl. Phys. B9, 331 (1969) and W. Kittel, L. Van Hove, and W. Wojcki, Report No. CERN/DPhII/Phys 70-8, 1970 (unpublished). The parameter b is actually given by $b^2 = [N/(N-1)]B^2$ where N is the number of particles. The factor $N/(N-1)$ is due to a δ function for momentum conservation: the average $p_\perp$ is con-

strained by forcing the sum of the transverse momenta to be zero. A more efficient event generator which was developed after GENIS is GENIUS [David C. Carey and Daniel Drijard, J. Comput. Phys. 28, 327 (1978); see also R. B. Chaffee, SLAC Computation Group Technical Memo No. 195, 1979 (unpublished)].

[12]V. Lüth *et al.*, Phys. Lett. 70B, 120 (1977).

[13]Y. S. Tsai, Phys. Rev. D 12, 3533 (1975).

[14]For a review of beam polarization in high-energy e^+e^- storage rings, see R. F. Schwitters, in *High Energy Physics with Polarized Beams and Polarized Targets,* proceedings of the Third International Symposium, Argonne, 1978, edited by G. H. Thomas (AIP, New York, 1978), p. 91. See also V. N. Baĭer, Usp. Fiz. Nauk. 105, 441 (1971) [Sov. Phys. Usp. 14, 695 (1972)]; and in *Physics with Storage Rings,* proceedings of the International School of Physics "Enrico Fermi," Varenna, 1969, Course XLVI, edited by B. Touschek (Academic Press, New York, 1971), pp. 1—49; and J. D. Jackson, Rev. Mod. Phys. 48, 417 (1976).

[15]I. M. Ternov, Yu. M. Loskutov, and L. I. Korovina, Zh. Eksp. Teor. 41, 1294 (1961) [Sov. Phys. JETP 14, 921 (1962)].

[16]A. A. Sokolov and I. M. Ternov, Dok. Akad. Nauk. SSSR 153, 1052 (1963) [Sov. Phys. Dokl. 8, 1203 (1964)].

[17]J. G. Learned, L. K. Resvanis, and C. M. Spencer, Phys. Rev. Lett. 35, 1688 (1975).

[18]R. F. Schwitters *et al.*, Phys. Rev. Lett. 35, 1320 (1975).

[19]G. Hanson, in *Gauge Theories and Leptons,* proceedings of the 13th Rencontre de Moriond, Les Arcs, France, edited by J. Trân Thanh Vân (Editions Frontieres, Dreux, France, 1979), p. 15.

[20]R. H. Schindler *et al.*, Phys. Rev. D 24, 78 (1981).

[21]M. Bardadin-Otwinowska *et al.*, Phys. Lett. 21, 351 (1966). Our data are compared with muoproduction in W. A. Loomis *et al.*, Phys. Rev. D 19, 2543 (1979).

[22]See, for example, G. Wolf, in *Proceedings of the XI International Symposium on Multiparticle Dynamics, Bruges, Belgium, 1980,* edited by E. De Wolf and F. Verbeure (Univ. Antwerp, Antwerp, Belgium, 1980), p. 283.